

Formation and Evolution of Self-Interacting Dark Matter Haloes

Kyungjin Ahn^{*} and Paul R. Shapiro[†]

Department of Astronomy, The University of Texas at Austin, 1 University Station C1400, Austin, TX 78712, USA

14 October 2018

ABSTRACT

We have derived the first, fully-cosmological, similarity solutions for cold dark matter (CDM) halo formation in the presence of nongravitational collisionality (i.e. elastic scattering), which provides an analytical theory of the effect of the self-interacting dark matter (SIDM) hypothesis on halo density profiles. Collisions transport heat inward which flattens the central cusp of the CDM density profile to produce a constant-density core, while continuous infall pumps energy into the halo to stabilize the core against gravothermal catastrophe. This is contrary to previous analyses based upon isolated haloes, which predict core collapse within a Hubble time. These solutions improve upon earlier attempts to model the formation and evolution of SIDM haloes, offer deeper insight than existing N-body experiments, and yield a more precise determination of the dependence of halo density profile on the value of the CDM self-interaction cross section. Different solutions arise for different values of the dimensionless collisionality parameter $Q \equiv \sigma \rho_b r_{\text{vir}} \propto r_{\text{vir}} / \lambda_{\text{mfp}}$, where σ is the scattering cross section per unit mass, ρ_b is the cosmic mean matter density, r_{vir} is halo virial radius and λ_{mfp} is the collision mean free path. The maximum flattening of central density occurs for an intermediate value of Q , Q_{th} , at which the halo is maximally relaxed to isothermality. The density profiles with constant-density cores preferred by dwarf and low surface brightness galaxy (LSB) rotation curves are best fit by the maximally-flattened ($Q = Q_{\text{th}}$) solution. If we assume that dwarfs and LSB galaxies formed at their typical collapse epoch in Λ CDM, then the value of σ which makes $Q = Q_{\text{th}}$ is $\sigma \simeq 200 \text{ cm}^2 \text{ g}^{-1}$, much higher than previous estimates, $\sigma \simeq [0.5 - 5] \text{ cm}^2 \text{ g}^{-1}$, based on N-body experiments. If σ is independent of collision velocity, then the same value $\sigma \simeq 200 \text{ cm}^2 \text{ g}^{-1}$ would make $Q > Q_{\text{th}}$ for clusters, which typically formed only recently, resulting in relatively less flattening of their central density profile and a smaller core.

Key words: cosmology: dark matter – cosmology: large-scale structure of universe – galaxies: kinematics and dynamics

1 INTRODUCTION

The cold dark matter (CDM) model provides a successful framework for understanding the formation and evolution of structure in our universe. According to this model, gravity amplifies primordial density fluctuations, and structure forms by hierarchical clustering: small objects form first, later merging to form larger objects. The most promising candidate for CDM is the weakly interacting massive particle (WIMP). In this picture, the microscopic interaction between CDM particles is negligible (collisionless), and they interact only by gravity. However, this assumption has not been fully verified and it is fair to say that the microscopic

nature of CDM is still unknown. It is important, therefore, to explore the consequences of varying this underlying assumption about CDM in the hope that astronomical observations can be used to place meaningful constraints.

The possible variation of the microscopic nature of cold dark matter is closely linked to the problems of the CDM model. Despite its success, the CDM model has several problems which exist mostly in the small scale regime (see, for example, Moore 2001). Among these problems, much attention has been focused on the N-body simulation results for the inner density slope, since the observed rotation curves of dark-matter dominated dwarf and low surface brightness (LSB) disk galaxies tend to favour mass profiles with a flat-density core unlike the singular profiles of the CDM N-body simulations (e.g. Flores & Primack 1994; Marchesini et al. 2002). The latter are generally characterized by an empirical fitting

^{*} Email: kjahn@astro.as.utexas.edu

[†] Email: shapiro@astro.as.utexas.edu

formula for the spherically averaged density profiles in those N-body results, either the Navarro-Frenk-White (NFW) profile (Navarro, Frenk & White 1997), for which $\rho \propto r^{-1}$ as $r \rightarrow 0$, or the Moore profile (Moore et al. 1999), for which $\rho \propto r^{-1.5}$ instead¹. It was controversial whether the observed data was resolved well enough to indicate a soft core (e.g. see van den Bosch & Swaters 2001 for possible beam smearing effect on the data), but observations have built up which favour the soft core even after eliminating the beam smearing effect (e.g. Marchesini et al. 2002 and references therein). After much more work on the N-body simulations of CDM, the discrepancy between these data and the numerical halo profiles remains significant (see, for instance, Diemand, Moore & Stadel 2004).

This apparent discrepancy between the N-body simulation results and observations of dwarf galaxy rotation curves has raised a question about the nature of dark matter, including the assumption that CDM is collisionless. People have suggested solutions to this discrepancy which either preserves the collisionless nature of the dark matter or else adopts a new picture. In the former category are explanations which attribute the discrepancy to astrophysical processes beyond the pure N-body dynamics (e.g. El-Zant, Shlosman & Hoffman 2001; Weinberg & Katz 2002) or to a primordial power spectrum tilted away from the Harrison-Zel'dovich shape (e.g. Zentner & Bullock 2002). In the latter category, the proposal of self-interacting dark matter (SIDM) by Spergel & Steinhardt (2000) has received a lot of attention. In this picture, microscopic interaction between dark matter particles is non-negligible and can affect the dynamics of halo formation. Since the actual identity and microscopic nature of CDM is still unknown, it is important to explore the consequences of such hypotheses in the hope that astronomical observations can be used to place meaningful constraints.

The truncated isothermal sphere (TIS) halo model developed by Shapiro, Iliev & Raga (1999, also see Iliev & Shapiro 2001) provides a simple physical clue about the existence of such soft cores in haloes of cosmological origin which otherwise closely resemble the CDM haloes found by N-body simulation in all respects except the presence of the inner cusp. The model is based upon the assumption that haloes form from the collapse and virialization of “top-hat” density perturbations and are spherical, isotropic, and isothermal. This leads to a unique, nonsingular TIS, a minimum-energy solution of the Lane-Emden equation. The resulting density profile is nearly indistinguishable from that deduced from the observed rotation curves of dwarf and LSB disk galaxies, as fit by Burkert (1995) with a profile involving a soft core (Iliev & Shapiro 2001). The assumption of isothermality which underlies the TIS

¹ Recently, Hayashi et al. (2004) and Navarro et al. (2004) reported that the logarithmic slope of the spherically averaged density profile of dark matter haloes in their Λ CDM simulations, $-\mathrm{d} \ln \rho / \mathrm{d} \ln r$, decreases monotonically towards the centre. This change of slope, however, does not seem to fully account for the observed rotation curves. Diemand, Moore & Stadel (2004) conclude, by surveying several simulation results by different groups, that neither the typical NFW profile nor the Moore profile provides a good fit, but one needs a little more complex form such as the one by Navarro et al. (2004).

halo model is the primary reason that the central cusp of the CDM N-body haloes is replaced by a soft core. The N-body haloes are also approximately isothermal, but there is typically a small temperature dip near the centre. This suggests that if some mechanism existed to transport heat inward so as to make CDM haloes more isothermal, they might exhibit soft cores while maintaining the same basic halo structure at larger radii already found for CDM haloes. The collisionality of SIDM serves as such a mechanism: elastic collisions transport heat inward, which flattens the central cusp of the CDM density profile to produce a constant-density core.

The problem of SIDM halo formation has so far been studied primarily by numerical N-body experiments. Some of the first attempts to calculate the effect of the elastic scattering of SIDM on halo structure formation involved *isolated* haloes which were assumed initially to follow the equilibrium profiles (e.g. NFW profile) found in collisionless N-body simulations of standard CDM (Burkert 2000; Kochanek & White 2001; both start from the Hernquist profile (Hernquist 1990) which is a good approximation to the NFW profile). Kochanek & White (2001), for instance, found that SIDM haloes can form flat density cores within a relaxation time as expected, but also that the lifetime of such flat cores is only a few relaxation times. They concluded, therefore, that most galactic haloes would have undergone core collapse.

The effect of SIDM collisionality on halo structure has also been studied by Balberg, Shapiro & Inagaki (2002, BSI hereafter) by solving 1D, quasi-static fluid equations. These authors also considered *isolated* haloes like those in the N-body experiments mentioned above, adopting 1D, spherical symmetry, with non-cosmological boundary conditions. They treated the dynamics of SIDM by a fluid approximation developed previously in the study of stellar dynamics, derived from the Boltzmann equation, in which they modified the heat conduction term to handle the elastic scattering of the SIDM particle-particle interaction. They solved the spherically-symmetric, virialized “gravothermal fluid” equations of Lynden-Bell & Eggleton (1980), which include mass conservation, hydrostatic equilibrium, an equation for heat conduction, and the first law of thermodynamics. According to these equations, the halo is time-dependent because heat conduction causes it to evolve through a continuous sequence of hydrostatic equilibria. An analytical self-similar solution to these equations was found in the limit of large scattering mean free path – the limit where the mean free path is much larger than the size of the halo – following the derivation of Lynden-Bell & Eggleton (1980) for globular clusters. The BSI solution shows that secular evolution always takes a configuration in the long mean free path limit and drives it into the short mean free path regime. In order to track the evolution into the short mean free path regime, as well, BSI then used their similarity solution as the initial condition for a numerical solution of the same gravothermal fluid equations, but for finite scattering cross-section. This approach made it possible to follow core collapse to a much more advanced stage than the N-body experiments could. From this, they concluded that the ultimate core collapse time was much larger than the relaxation time in the core, long enough even to exceed a Hubble time in some

cases². Their estimated core collapse time is $t_{\text{coll}} \simeq 290 t_r$, which contradicts the result found by Burkert (2000) and Kochanek & White (2001) that the core collapse time was only a few relaxation times.

This apparent discrepancy in core collapse timescale between the study by BSI and the numerical N-body experiments (Burkert 2000; Kochanek & White 2001) may be attributed to the fact that their adopted initial conditions were different. In BSI, as mentioned, the initial condition was tuned to be in the extremely long mean free path limit, $\lambda_{\text{mfp}}/H \gg 1$, where λ_{mfp} is the mean free path and H is the gravitational scale height or roughly the halo size. This occurs when the system is either dilute enough or the scattering cross section (per unit mass) σ is small enough, since $\lambda_{\text{mfp}} \propto 1/(\sigma\rho)$. According to BSI, most of the collapse time is spent to reach the condition $\lambda_{\text{mfp}}/H \simeq 1$, and the halo density profile always has a flat core. By contrast, Kochanek & White (2001) started with a cuspy profile with parameters which corresponded to a condition $\lambda_{\text{mfp}}/H \simeq 0.1-3.0$. In this case, SIDM halo cores can quickly reach $\lambda_{\text{mfp}}/H \simeq 1$ or they are already in the short mean free path limit, which then requires only a few relaxation times for core collapse.

In what follows, we will cover the whole range of σ and show that the observed dwarf-galaxy rotation curves are best-fit when the SIDM interaction has its maximal effect, which occurs when $\lambda_{\text{mfp}}/H \simeq 1$, so the regime of greatest interest may be that of Kochanek & White (2001). If so, then most isolated haloes would, indeed, suffer core collapse within a Hubble time. However, the shared limitation of the analyses of BSI, Burkert (2000) and Kochanek & White (2001), that of non-cosmological boundary conditions, is a severe one. Cosmological infall may inhibit core collapse. If cosmological infall can delay core collapse substantially, previous estimates based on isolated halo models would change by shifting the time of the onset of core collapse until cosmological infall becomes negligible.

The effect of cosmological boundary conditions on SIDM halo formation has been studied numerically by cosmological N-body simulations, in which Gaussian random noise initial conditions for CDM were incorporated. Early work along these lines attempted to derive the maximal effect of collisionality by adopting the fully collisional limit which corresponds to ordinary gas dynamics (Yoshida et al. 2000a; Moore et al. 2000). The surprising result they reported was that simulations yielded density profiles with central cusps even steeper – with logarithmic slope close to -2 – than those in collisionless N-body simulations. Subsequent cosmological N-body experiments which treated the SIDM elastic scattering in more detail, however, reported that halo density profiles were flatter than those of either fully collisional or purely collisionless simulations (Yoshida et al. 2000b; Davé et al. 2001; Colín et al. 2002). They found that values of σ in the range $\sigma \simeq [0.1-5] \text{ cm}^2 \text{ g}^{-1}$ (the range of preferred σ varies among these works, but within less than an order of magnitude) produced SIDM haloes with sufficient profile flattening to account for dwarf

galaxy rotation curves, which did not suffer from the rapid core collapse identified in the earlier N-body experiments for isolated haloes. Davé et al. (2001) speculated that this might be the result of cosmological infall, which was absent from the calculations of isolated haloes. In addition, Yoshida et al. (2000b) found that SIDM collisions in cluster-sized haloes would be more frequent than in dwarf-sized haloes, thus producing relatively larger cores in clusters, while observations tend to show that dwarfs and LSBs show relatively larger cores than clusters. This led them to suggest that the scattering cross section be velocity-dependent ($\sigma \propto 1/v$) so that more massive haloes would have a smaller degree of density profile flattening. Later, Colín et al. (2002) tested this hypothesis and confirmed that it could match observed core sizes from dwarfs to galaxy clusters.

Further study of the formation and evolution of SIDM haloes is warranted to resolve the issues raised by previous work and put the subject on a firmer theoretical footing. On the one hand, the numerical N-body simulations and 1D semi-analytical treatment mentioned above of isolated haloes with non-cosmological boundary conditions are unable to address the important effects of cosmological infall. On the other hand, the fully cosmological N-body simulations which have been performed of haloes that arise during large-scale structure formation in the SIDM model have so far been limited by numerical resolution and dynamic range. As a result, simulation results published to date do not attempt a detailed enough comparison with observed galactic rotation curves to determine if SIDM haloes can really match them or to give a very reliable constraint on the SIDM cross section. Such simulations do not afford enough insight into the underlying dynamical processes which govern the halo structure, either. Finally, the wide range of typical collapse epochs expected in a CDM universe for the wide range of halo masses extending from dwarf galaxies to clusters suggests that the effect of the SIDM interaction may be halo-mass-dependent; this dependence has not yet been adequately explored.

Towards this end, we have derived a fully cosmological model for the origin and evolution of CDM haloes in the presence of nongravitational collisionality (i.e. elastic scattering). We have combined the fluid approximation of BSI with the spherical infall model for cosmological perturbation growth to yield fully time-dependent, detailed similarity solutions for SIDM haloes, for arbitrary degree of collisionality. We shall apply these solutions to test the hypothesis that cosmological infall retards the core collapse of SIDM haloes, and compare the predicted SIDM halo profiles with the mass profiles inferred from dwarf galaxy rotation curves. This will enable us to place much better quantitative constraints on the SIDM cross section and better assess the validity of the SIDM model.

Subsequent to the original suggestion by Spergel & Steinhardt (2000) and the exploration described above of the halo structure which results, related work has focused on constraining the SIDM hypothesis by its implications for other astrophysical phenomena or attributing density flattening to more complicated CDM dynamics or gas dynamical feedback effects within the standard CDM picture. There seem to be strong observational constraints on the possible range of σ . Gnedin & Ostriker (2001) ruled out a range of σ , $\sigma = [0.3 - 10^4] \text{ cm}^2 \text{ g}^{-1}$,

² In a follow-up paper, the authors showed how this process could lead to the formation of seeds for super-massive black holes (Balberg & Shapiro 2002).

based on their calculation of the evaporation time of the dark matter haloes of elliptical galaxies in the clusters. Natarajan et al. (2002) rule out all values of $\sigma > 42 \text{ cm}^2 \text{ g}^{-1}$ by comparing the predicted truncation radii of SIDM haloes inside clusters by ram-pressure stripping to those of observed haloes which they obtain using cluster gravitational lensing observations. Hennawi & Ostriker (2002) conclude that if $\sigma \gg 0.02 \text{ cm}^2 \text{ g}^{-1}$, the supermassive black holes in the centres of galactic haloes would be more massive than observed. Along the line of explaining flattened cores within the standard CDM picture (see Primack 2003 for recent review), El-Zant et al. (2004), as in El-Zant, Shlosman & Hoffman (2001), investigate the effect of dynamical friction by clumpy substructure associated with baryonic dissipation and show that a flat core can be generated. Weinberg & Katz (2002) and Holley-Bockelmann, Weinberg & Katz (2003) claim that soft cores can be induced by the presence of a CDM bar structure. Hayashi et al. (2004) argue that the gas rotation speed in a galactic disk may be different from the dark matter circular velocity, which would, therefore, be wrongfully interpreted as implying the existence of soft cores. Dynamical feedback effects from supernova explosions is another possibility (Navarro, Eke & Frenk 1997). Observationally, related to the missing satellite problem, the gravitational lensing flux anomaly seems to require clumpy, dark substructures (Metcalf & Zhao 2002; Dalal & Kochanek 2002; Keeton, Gaudi & Petters 2003; Mao et al. 2004), even though no firm conclusion has been established yet.

Nevertheless, we believe that SIDM is still a viable candidate for dark matter. As we shall discuss below in §6, the previous analyses restricting σ are subject to significant caveats. It is meaningful to study this subject because it can shed light on the nature of dark matter whose origin we do not know yet, and simply because CDM problems are far from reaching a firm conclusion. Also, the research effort on SIDM has not yet reached the level of that on collisionless CDM.

We have previously reported the results of this paper in a summarized form elsewhere. Ahn & Shapiro (2003a,b) briefly described the result from §5.5.2. Shapiro et al. (2004) summarized the results in light of the current status of CDM research. However, we warn the reader that these works should be considered as guidelines to the detailed, complete picture of this paper.

The plan of this paper is as follows. In §2, we review the previous work on self-similar gravitational collapse in the spherical infall model. In §3, we show how the fluid approximation derived from the Boltzmann equation can be generalized to include a conduction term which accounts for nongravitational collisionality in an otherwise collisionless dark matter gas. The assumptions which underlie this fluid approximation will be justified by comparison with the results of cosmological N-body simulations of CDM haloes and with detailed similarity solutions for halo formation by gravitational collapse of collisionless dark matter. In §4, we show that gravitational collapse by spherical infall can be self-similar even in the presence of collisionality, and that the specific condition required for self-similarity is relevant to galactic haloes. We then describe the basic equations for the dynamics of SIDM haloes. In §5, we present the simi-

larity solution and its application to test the SIDM hypothesis, including a comparison with previous N-body results and observed galactic rotation curves. Our conclusions and discussion are in §6.

2 SELF-SIMILAR GRAVITATIONAL COLLAPSE

2.1 Previous analytical models for halo formation: the spherical infall model

Analytical approximations have been developed to model the formation of haloes by the 1D growth of spherical cosmological density perturbations, in either a collisionless gas or a fluid. We shall need to refer to some of these solutions to justify our fluid approximation in §3. We shall also build upon these earlier solutions in deriving new ones which add the effects of collisionality in §3.2 and 4. It is necessary for us to begin, therefore, by briefly recounting this earlier work.

Gunn & Gott (1972) first presented the concept of the so called “secondary infall model (SIM)”. This SIM refers to the effect of the addition of a point mass to a uniform, expanding Friedmann–Robertson–Walker universe as a perturbation which causes the surrounding spherical shells to decelerate relative to the background universe, until they reach a radius of maximum expansion and re-collapse. Subsequent work generalized this approach to include spherically-symmetric initial perturbations for which the overdensity profile depends upon radius or mass as a scale-free power-law. Along these lines, Fillmore & Goldreich (1984, FG hereafter) studied the dynamics of collisionless CDM haloes using a self-similar model, adopting a scale-free initial overdensity parametrized by its shape: ε in equation (1). Bertschinger (1985) studied a special case of FG but also extended the analysis to a collisional fluid. Hoffman & Shaham (1985, HS hereafter) showed that a power-law power spectrum would indeed generate a scale-free initial condition, such as was adopted by FG. They then argued that the resulting nonlinear structure would be described by a power-law profile determined by the shape of the power spectrum.

Previously mentioned works adopted a rather unrealistic condition for the collisionless case, that of purely radial motion. N-body simulations of CDM halo formation find that the virialized region tends toward isotropic random velocities. Some attempts to incorporate tangential velocities within the framework of spherical symmetry have also been made by Ryden & Gunn (1984), Avila-Rees, Firmani & Hernández (1998) and Hozumi, Burkert & Fujiwara (2000). Along these lines, one may also refer to work by Kull (1999), Lokas & Hoffman (2000), Del Popolo et al. (2000), Hiotelis (2002) and references therein.

The fluid approximation of collisionless CDM halo formation has emerged recently. Teyssier, Chieze & Alimi (1997) showed that one could use fluid-like conservation equations to mimic the radial-only SIMs such as the FG model. Subramanian, Cen & Ostriker (2000) extended this analysis to include tangential motion. In these pictures, one could expect, for instance, accretion shock structure. Teyssier, Chieze & Alimi (1997) and Subramanian, Cen & Ostriker (2000) therefore used a

“shock jump condition” which one would only expect from a purely collisional fluid. The fluid approximation has been used in the literature of stellar dynamics, but its application to CDM halo dynamics is rather new, and as will be described in §3, it simplifies the description of dark matter dynamics substantially.

Self-similar spherical infall models have also been used to study the effect of incorporating additional baryonic physics. Bertschinger (1989), Owen, Weinberg & Villumsen (1998), and Abadi, Bower & Navarro (2000) have studied the effect of gas cooling on galaxy formation using self-similar models. Because the system was tuned to maintain self-similarity in the presence of cooling, the cooling function used is not perfectly physical. Nevertheless, as shown by Abadi, Bower & Navarro (2000), one can use these models at least to test hydrodynamic codes in the presence of cooling. Moreover, these models capture the generic behaviour of galactic dynamics in the presence of realistic cooling.

The similarity model we shall develop in this paper is the first self-similar halo model which includes the effective heat conduction resulting from SIDM collisionality. In section §2.2 and 2.3, we describe how SIMs with scale-free linear perturbations arise naturally from the Gaussian random noise primordial density fluctuations, thus leading to the self-similar evolution of nonlinear structures.

2.2 Halo formation from scale-free linear perturbations

In the Einstein-de Sitter (EdS) background universe, an initial linear perturbation whose mass profile is spherically symmetric and has a scale-free, power-law form

$$\frac{\delta M}{M} \propto M^{-\varepsilon} \quad (1)$$

results in structure formation which is self-similar (FG). Each spherical mass shell around the centre expands until it reaches a maximum radius (turnaround radius r_{ta}), and re-collapses. For a given ε , we have

$$r_{\text{ta}} \propto t^{\xi}, \quad (2)$$

where

$$\xi = \frac{2}{3} \left(\frac{3\varepsilon + 1}{3\varepsilon} \right). \quad (3)$$

Since there are no characteristic length or time scales for this problem other than the turn-around radius r_{ta} and the Hubble time t , the gravitational collapse which ensues from this scale-free initial condition must be self-similar as long as the background universe is Einstein-de Sitter, in the absence of physical processes which introduce additional scales (e.g. SIDM collisionality)

In general, if the unperturbed matter is a cold fluid, the infall which results from this perturbation is highly supersonic and is terminated by a strong accretion shock which thermalizes the kinetic energy of collapse. The accretion shock radius is guaranteed by self-similarity to be a fixed fraction of $r_{\text{ta}}(t)$ at all times. The mean density of the postshock region is, therefore, always a fixed multiple of the cosmic mean matter density. For most cases of interest, this postshock region is close to hydrostatic. For a collisionless gas, a similar description applies as long as the infalling matter initially had small (or zero) random motions.

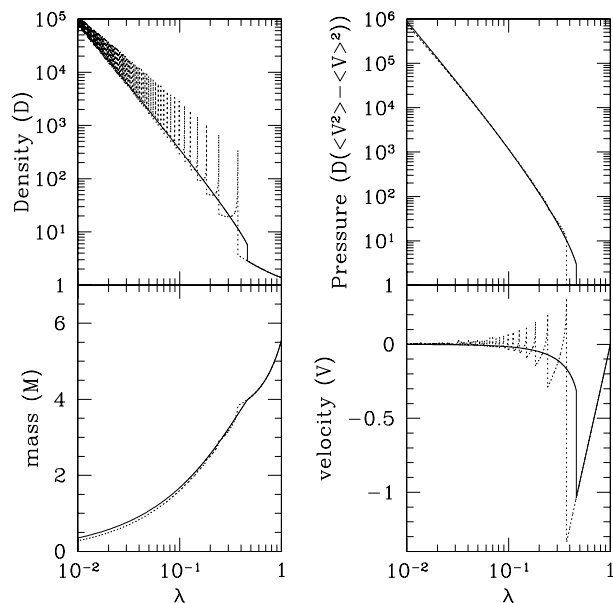


Figure 1. Self-similar collisionless halo formation for $\varepsilon = 1$: Comparison of the skewless-fluid approximation to the exact collisionless Bertschinger solution. Solid lines represent the solution obtained from the fluid approximation in the radial direction, while dotted lines represent the collisionless Bertschinger solution. Spikes in the density plot simply represent infinite values, corresponding to caustics, and therefore there is no physical significance in the height of these spikes. However, spikes in the velocity plot are finite and real. Note that solid lines do not represent the $\gamma = 5/3$ fluid Bertschinger solution.

In that case, each mass shell collapses supersonically as a single stream until it encounters a region of shell-crossing and density caustics, which encompasses all previously collapsed (i.e. interior) mass shells. All collapsed mass shells inside this region oscillate about the centre. The radius of this region of shell-crossing, given by the outermost density caustic, is analogous to the shock radius in the fluid case.

Results for the purely collisionless case were presented for arbitrary values of ε by FG, and for $\varepsilon = 1$ by Bertschinger (1985) (where the latter included a fluid component, as well). Figures 1 and 2 show the exact similarity solutions for the purely collisionless cases with $\varepsilon = 1$ and $\varepsilon = 1/6$, respectively. As we describe below in §2.3, these values roughly bracket the range relevant to cosmological haloes in a CDM universe. We will refer to these solutions again for comparison in deriving our fluid approximation in §3.

2.3 Halo formation from peaks of the Gaussian random noise primordial density fluctuations

The theory of halo formation from peaks in the density field which result from Gaussian-random-noise initial density fluctuations draws an interesting connection between the average density profile around these peaks and the shape of the fluctuation power spectrum. According to HS, local maxima of Gaussian random fluctuations in the density can serve as the progenitors of cosmological structures. They

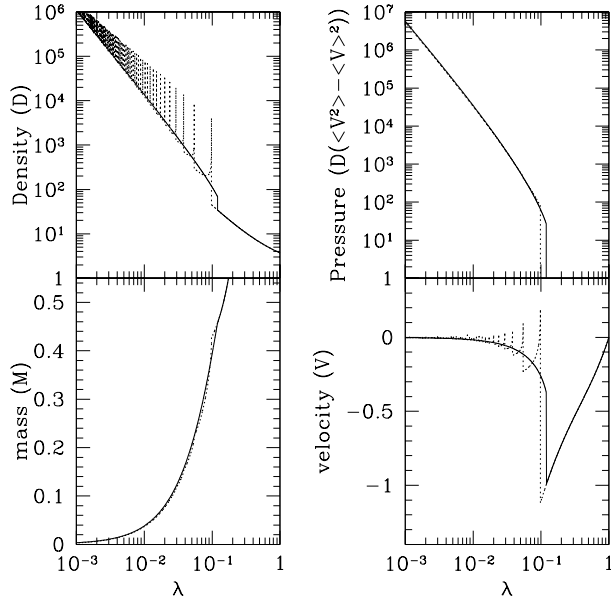


Figure 2. Same as Figure 1, but $\varepsilon = 1/6$. Note again that the solid line was not generated from the $\gamma = 5/3$ fluid approximation, but rather from the radial-only fluid approximation described by equations (22) - (24).

show that rare density peaks ($\nu \geq 3$, where ν corresponds to $\nu\sigma_M$ peak) have a simple power-law profile³

$$\Delta_0(r) \propto r^{-(n+3)}, \quad (4)$$

where $\Delta_0(r)$ is the accumulated overdensity inside radius r , and n is the effective index of the power spectrum $P(k)$ approximated as a power-law $P(k) \propto k^n$ at wavenumber k which corresponds to the halo mass as described in Appendix⁴. The overdensity $\Delta_0(r)$ is equivalent to the fractional mass perturbation $\delta M/M$ inside radius r ,

$$\Delta_0(r) = \delta M/M \propto M^{-\frac{n+3}{3}}. \quad (5)$$

From equations (1) and (5), we deduce that the power-law power spectrum naturally generates a scale-free initial condition with

$$\varepsilon = (n + 3)/3. \quad (6)$$

According to this model, as described in Appendix, haloes of a given mass M originate from density perturbations given by equation (5) with n determined by the primordial power spectrum after it is transferred according to the parameters of the background universe and the nature of the dark matter. We plot this effective n as a function of halo mass in Figure 3 for the current Λ CDM universe. The value of $n \simeq -2.5$ is a reasonable approximation for galactic haloes (i.e. $n \simeq -2.5 \pm 0.1$ for $M \simeq 10^{8 \pm 2} M_\odot$, while $n \simeq -2.5 \pm 0.2$

³ Bardeen et al. (1986) also get a similar result: local density maxima have a triaxial profile, but as ν increases it becomes more and more spherical with a profile converging to equation (4).

⁴ The average linear overdensity profile, equation (4), holds for any value of ν . For small ν , however, random dispersion around this average profile becomes substantial, limiting the generality of equation (4).

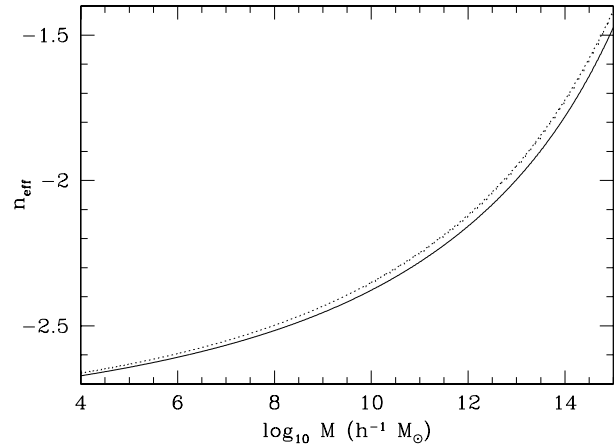


Figure 3. Effective index of the power spectrum ($P(k) \propto k^{n_{\text{eff}}}$) vs. halo mass for the Λ CDM universe. Appendix describes how n_{eff} is calculated. The solid line is derived from the HS approach, which we use in this paper. The dotted line is derived from σ_M .

for M in the range from $10^3 M_\odot$ to $10^{11} M_\odot$). For haloes in the cluster mass range, $M \sim 10^{15} M_\odot$, $n \simeq -1.5$.

3 FLUID APPROXIMATION OF DARK MATTER DYNAMICS

We show that fluid conservation equations for a gas with adiabatic index $\gamma = 5/3$ are a good approximation to the dynamics of both CDM and SIDM haloes. This approach has been used in the literature of stellar dynamics (e.g. Larson 1970; Lynden-Bell & Eggleton 1980; Bettwieser 1983) for the study of the gravothermal catastrophe, where particles (stars) experience gravitational two-body interactions. The authors integrated the Boltzmann equation with a collision term due to gravitational two-body interactions, to obtain a set of moment equations. They then truncated, under reasonable assumptions, the hierarchy of such moment equations such that only fluid-like conservation equations remain. The effect of gravitational two-body interactions was naturally approximated as an effective heat conduction. In the CDM literature, Teyssier, Chieze & Alimi (1997) and Subramanian, Cen & Ostriker (2000) followed a similar approach for the study of CDM haloes. Contrary to systems described by stellar dynamics where the number of particles is small, gravitational two-body interactions are completely negligible for CDM haloes. The authors integrated collisionless Boltzmann equation to obtain a set of moment equations, and truncated its hierarchy as done for stellar dynamics. This results in fluid conservation equations for collisionless systems. This idea may bother some readers since, strictly speaking, the collisionless nature of CDM prohibits the use of such an approximation. Collisionless particles have, in principle, an infinite set of moment equations when the Boltzmann equation is integrated (BBGKY hierarchy; e.g. Binney & Tremaine 1987). However, a couple of simple assumptions enable us to treat CDM halo dynamics with the usual fluid conservation equations. This section is devoted to the derivation of the fluid approximation, which

we will use in §4 to obtain self-similar equations both for the collisionless CDM and the collisional SIDM halo formation and evolution.

Alvarez, Ahn & Shapiro (2003) have already applied this formalism to study CDM halo formation. Adopting the universal mass growth history reported for CDM N-body haloes (e.g. Wechsler et al. 2002) and applying the fluid approximation, they have shown that the resulting shape of the equilibrium halo profile and its evolution match those of CDM N-body simulations remarkably well. In addition to this convincing result, we shall also justify the fluid approximation in §3.1.

We develop this model under certain conditions. First, spherical symmetry is assumed. The initial condition is given by a spherically symmetric overdense region, and the subsequent evolution does not break the symmetry. Second, the infall of matter is assumed to be continuous. This can be achieved if we assume a smooth initial overdensity profile. Third, we restrict our attention to the matter-dominated era such that the cosmic mean density $\rho_b \propto t^{-2}$. This condition is true in the Λ CDM universe if the redshift is restricted to be $1 \lesssim z \lesssim z_{\text{eq}}$, where z_{eq} is the redshift for the matter-radiation equality.

3.1 Fluid approximation of collisionless CDM dynamics

Let us describe the fluid approximation for a self-gravitating, weakly collisional system in spherical symmetry. We define the average physical quantities as follows:

$$\rho = \int f d^3v, \quad (7)$$

$$\langle A \rangle \equiv \frac{\int A f d^3v}{\int f d^3v} = \frac{1}{\rho} \int A f d^3v, \quad (8)$$

$$u \equiv \langle v_r \rangle, \quad (9)$$

$$p_r \equiv \rho \langle (v_r - \langle v_r \rangle)^2 \rangle, \quad (10)$$

$$p_\theta \equiv \rho \langle (v_\theta - \langle v_\theta \rangle)^2 \rangle = \rho \langle v_\theta^2 \rangle, \quad (11)$$

$$p_\phi \equiv \rho \langle (v_\phi - \langle v_\phi \rangle)^2 \rangle = \rho \langle v_\phi^2 \rangle, \quad (12)$$

where f is the distribution function defined such that $f(\mathbf{r}, \mathbf{v}) d^3r d^3v$ = mass within infinitesimal volume $d^3r d^3v$ at (\mathbf{r}, \mathbf{v}) , ρ is the density, $\langle A \rangle$ is the average value of a certain quantity A , u is the radial bulk velocity, p_r is the “effective radial pressure”, and p_θ is the “effective tangential pressure”. Note that $\langle v_\theta \rangle = \langle v_\phi \rangle = 0$ and $p_\theta = p_\phi$ because of spherical symmetry. Anisotropy in the velocity dispersion occurs in general – i.e. $p_r \neq p_\theta$ or anisotropy parameter $\beta \neq 0$ where $\beta \equiv 1 - \frac{p_\theta}{p_r}$ – implying that we should treat p_r and p_θ separately. In a highly collisional system, which is well described by fluid conservation equations, $p_r = p_\theta$ and the usual pressure $p = p_r = p_\theta$.

A self-gravitating system of collisionless particles can be described by the collisionless Boltzmann equation

$$\frac{df}{dt} = 0, \quad (13)$$

where $\frac{d}{dt}$ is the phase-space Lagrangian time-derivative, given by

$$\frac{d}{dt} = \frac{\partial}{\partial t} + \mathbf{v} \cdot \frac{\partial}{\partial \mathbf{r}} + \mathbf{a} \cdot \frac{\partial}{\partial \mathbf{v}}. \quad (14)$$

Throughout this paper, we will use the Newtonian approximation: when a system is much larger than its Schwarzschild radius and much smaller than the horizon size, motions of particles and the temperature of the system become non-relativistic. In this limit, we can use the non-relativistic Boltzmann transport equation. This equation can then be written more explicitly in spherical coordinates. For a system in spherical symmetry, $f = f(|\mathbf{r}|, \mathbf{v})$, and equation (13) reads

$$\begin{aligned} 0 = & \frac{\partial f}{\partial t} + v_r \frac{\partial f}{\partial r} + \left(\frac{v_\theta^2 + v_\phi^2}{r} - \frac{\partial \Phi}{\partial r} \right) \frac{\partial f}{\partial v_r} \\ & + \frac{1}{r} (v_\phi^2 \cot \theta - v_r v_\theta) \frac{\partial f}{\partial v_\theta} \\ & - \frac{v_\phi}{r} (v_r + v_\theta \cot \theta) \frac{\partial f}{\partial v_\phi}, \end{aligned} \quad (15)$$

where Φ satisfies the Poisson equation $\nabla^2 \Phi = 4\pi G \rho$ (Binney & Tremaine 1987). By multiplying equation (15) by $\int d^3v v_r^m v_\theta^n$, where m, n are integer numbers, we can form a set of moment equations. Moment equations from the lowest order are

$$\frac{\partial \rho}{\partial t} + \frac{\partial}{\partial r} (r^2 \rho u) = 0, \quad (16)$$

$$\frac{\partial}{\partial t} (\rho u) + \frac{\partial}{\partial r} (p_r + \rho u^2) + \frac{2}{r} (p_r - p_\theta + \rho u^2) = -\rho \frac{Gm}{r^2}, \quad (17)$$

$$\rho \frac{D}{Dt} \left(\frac{p_r}{2\rho} \right) + p_r \frac{\partial u}{\partial r} = \Gamma_1, \quad (18)$$

$$\rho \frac{D}{Dt} \left(\frac{p_\theta}{2\rho} \right) + \frac{p_\theta u}{r} = \Gamma_2, \quad (19)$$

⋮

where m is the mass enclosed by a shell at radius r , $\frac{D}{Dt} \equiv \frac{\partial}{\partial t} + u \frac{\partial}{\partial r}$, and

$$\begin{aligned} \Gamma_1 = & \frac{\rho}{r} \langle 2(v_r - \langle v_r \rangle) v_\theta^2 \rangle \\ & - \frac{1}{2r^2} \frac{\partial}{\partial r} (r^2 \rho \langle (v_r - \langle v_r \rangle)^3 \rangle), \end{aligned} \quad (20)$$

$$\Gamma_2 = -\frac{1}{4r^4} \frac{\partial}{\partial r} (r^4 \rho \langle (v_r - \langle v_r \rangle) v_\theta^2 \rangle). \quad (21)$$

Equations (16) - (19) are conservation equations of mass, momentum, “radial” energy, and angular momentum respectively. Note that equations (16) - (21) are all in exact form, and the hierarchy of equations is not closed in principle.

Now we make a further simplification that the distribution of v_r is skewless – v_θ and v_ϕ are naturally skewless because of spherical symmetry. In other words, we assume that v_r has a symmetric distribution around $\langle v_r \rangle$. It is not straightforward to show that Γ_1 and Γ_2 are negligible in equations (18) and (19). However, we demonstrate that the assumption of “skewlessness” in the fluid approximation yields results which are in good agreement with the purely collisionless CDM structure, for specific examples⁵.

⁵ Subramanian, Cen & Ostriker (2000) argue that an initially skewless distribution function f will remain skewless even after

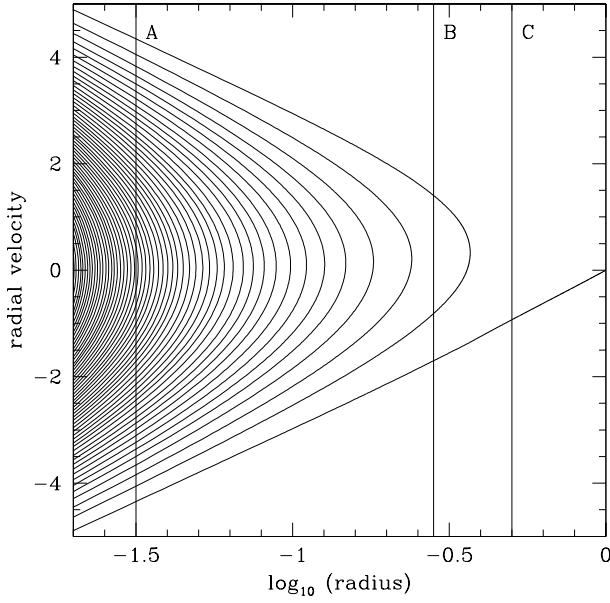


Figure 4. Self-similar collisionless halo formation for $\varepsilon = 1$: Phase-space diagram of Bertschinger (1985) solution as an illustration of the “skewless distribution” assumption. Along the line A there are a large number of shell-crossings, which are almost symmetric around $\langle v_r \rangle$, and along the line C, as there is only one stream line, it is intrinsically skewless. On the contrary, there are only three stream lines along the line B, so the assumption is not good in the region inside and close to the outermost caustics. Tangential velocity distribution would have a similar behaviour when tangential motion is allowed.

As shown in the Bertschinger (1985) solution, for instance, collisionless particles (shells) form a quasi-symmetric winding structure in the phase space as shown in Figure 4. This indicates that we may neglect terms which arise as a result of skewness. Equations (16) - (18) with the condition $p_\theta = 0$ and $\Gamma_1 = \Gamma_2 = 0$,

$$\frac{\partial \rho}{\partial t} + \frac{\partial}{\partial r}(r^2(\rho u)) = 0, \quad (22)$$

$$\frac{\partial}{\partial t}(\rho u) + \frac{\partial}{\partial r}(p_r + \rho u^2) + \frac{2}{r}(p_r + \rho u^2) = -\rho \frac{Gm}{r^2}, \quad (23)$$

$$\rho \frac{D}{Dt} \left(\frac{p_r}{2\rho} \right) + p_r \frac{\partial u}{\partial r} = 0, \quad (24)$$

can be used to solve purely radial problems, such as the spherical infall problems with similarity solutions by Bertschinger (1985, $\varepsilon = 1$) and Fillmore & Goldreich (1984, with $\varepsilon = 1/6$). As seen in Figure 1, the solution to equations (22) - (24) is in good agreement with the true solution. We have also found, as seen in Figure 2, an excellent agreement between the collisionless solution and the one produced by a radial fluid approximation in the case of $\varepsilon = 1/6$ (the

evolution. It is true if one is interested in the fine-grained distribution, or each stream line. However, if one considers coarse-grained quantities as defined by equation (8), the contribution from multiple stream lines should be counted and the overall distribution is not skewless, in general.

$\varepsilon = 1/6$ case is of main interest in this paper). The difference observed at caustics – places where the density becomes infinite – is negligible, because caustics do not affect the overall dynamics of the halo. Since the skew-free assumption naturally neglects dynamically unimportant structure (e.g. caustics) while accurately reproducing the profile of the exact solution in these radial cases, it may also be applied to describe CDM haloes, in which particles have a tangential motion as well.

The final assumption is that inside the virialized structure (i.e. postshock region) the velocity dispersion is isotropic, or $p_r = p_\theta$. This is an empirical assumption: CDM haloes in cosmological N-body simulations show mild anisotropy. For instance, Carlberg et al. (1997) show that CDM haloes in their numerical simulation can be well-fitted by a fitting formula

$$\beta(r) = \beta_m \frac{4r}{r^2 + 4}, \quad (25)$$

where r is in units of r_{200} , and $\beta_m = [0.3 - 0.5]$ (see also, e.g., Thomas et al. 1998 and Colín, Klypin & Kravtsov 2000). As we will show in the following sections, our similarity solutions have a virial radius $r_{564} \simeq 0.6 r_{200}$, which then results in the maximum anisotropy $\beta \sim [0.17 - 0.28]$. This fact enables us to use $\beta = 0$ to a good approximation.

With these assumptions (spherical symmetry, skew-free velocity distribution, and isotropic velocity dispersion), the usual fluid conservation equations are obtained. They are

$$\frac{\partial \rho}{\partial t} + \frac{\partial}{\partial r}(r^2(\rho u)) = 0, \quad (26)$$

$$\frac{\partial}{\partial t}(\rho u) + \frac{\partial}{\partial r}(p + \rho u^2) + \frac{2}{r}\rho u^2 = -\rho \frac{Gm}{r^2}, \quad (27)$$

$$\frac{D}{Dt} \left(\frac{3p}{2\rho} \right) = -\frac{p}{\rho} \frac{\partial}{\partial r}(r^2 u), \quad (28)$$

which are identical to the fluid conservation equations for a $\gamma = 5/3$ gas in spherical symmetry. Resemblance of these equations to fluid equations indicate that we can expect an effective “shock” even for a collisionless system because of the hyperbolicity of these equations. This is also illustrated in Figure 4. For instance, the density jump occurs when one moves from the “pre-shock” region (line C; one stream line) to the “post-shock” region (line B; three stream lines). However, one should be careful in using this formalism because the approximation becomes worse where there are only a small number of phase-space windings.

3.2 Fluid approximation of SIDM haloes

We now consider the effect of SIDM collisionality. We adopt a simple, heuristic approach to account for the heat conduction as a result of finite cross-section. This will change the energy conservation equation (equ. [28]) to

$$\frac{D}{Dt} \left(\frac{3p}{2\rho} \right) = -\frac{p}{\rho} \frac{\partial}{\partial r}(r^2 u) - \nabla \cdot \mathbf{f}, \quad (29)$$

where \mathbf{f} is the heat flux.

The heat flux resulting from SIDM interaction has been derived by BSI. We briefly describe its derivation. When the scattering mean free path is much smaller than the system size (short mean free path limit, or diffusion limit), the heat flux (equivalent to $\frac{L}{4\pi r^2}$ in BSI) reads

$$\mathbf{f}_{\text{smfp}} = -\frac{3b}{2\sigma} \sqrt{\frac{p}{\rho}} \frac{\partial}{\partial r} \left(\frac{p}{\rho} \right) \hat{r}, \quad (30)$$

where b is an effective impact parameter of order unity, which is 1.002 for elastic scattering of hard spheres. On the contrary, when the mean free path is much larger than the system size (long mean free path limit), the proper length scale of heat transfer is not the mean free path (a multiple of the system size) but the system size, while the time scale is still the relaxation time. This results in

$$\mathbf{f}_{\text{lmfp}} = -\frac{3}{2} ab\sigma \sqrt{\frac{p}{\rho}} \frac{p}{4\pi G} \frac{\partial}{\partial r} \left(\frac{p}{\rho} \right) \hat{r}, \quad (31)$$

where $a = 2.26$ for elastic scattering of hard spheres.

In the end, we use a hybrid expression which is roughly valid in the intermediate regime as well as in two extreme regimes (short mean free path limit and long mean free path limit)⁶,

$$\mathbf{f} = -\frac{3}{2} ab\sigma \sqrt{\frac{p}{\rho}} \left(a\sigma^2 + \frac{4\pi G}{p} \right)^{-1} \frac{\partial}{\partial r} \left(\frac{p}{\rho} \right) \hat{r}. \quad (32)$$

Throughout this paper, we adopt $a = 2.26$ and $b = 1.002$.

3.3 Shock jump conditions

As we have shown in previous sections, fluid conservation equations can be used and we expect an accretion ‘‘shock’’ to occur. Across the shock, the matter, momentum and energy fluxes should all be continuous. Mathematically, a flux is a term acted upon by $\frac{\partial}{\partial r}$ in the conservation equations expressed in Eulerian coordinates.

In the adiabatic case⁷, therefore, we obtain the usual adiabatic shock jump conditions from equations (26) - (28):

$$[\rho \bar{u}] = 0, \quad (33)$$

$$[p + \rho \bar{u}^2] = 0, \quad (34)$$

$$\left[\rho \bar{u} \left(\frac{3p}{2\rho} + \frac{1}{2} \bar{u}^2 + \frac{p}{\rho} \right) \right] = 0, \quad (35)$$

where $[A] \equiv A(\text{preshock}) - A(\text{postshock})$, \bar{u} ($= u - u_s$) is the bulk radial velocity in the shock frame, and equation (35) comes from equation (28) if expressed in Eulerian coordinates by converting $\frac{D}{Dt}$ into $\frac{\partial}{\partial t} + u \frac{\partial}{\partial r}$.

For an SIDM case, as the heat conduction is included, the energy jump condition will instead be

$$\left[\rho \bar{u} \left(\frac{3p}{2\rho} + \frac{1}{2} \bar{u}^2 + \frac{p}{\rho} + f \right) \right] = 0, \quad (36)$$

where $\mathbf{f} = f \hat{r}$.

⁶ Note that the intermediate regime described by equation (32) is indeed a mere interpolation of two different regimes. We believe, however, that this is a good approximation: the intermediate value should not be too different from this smooth and continuous interpolation of two regimes.

⁷ We will use the term ‘‘adiabatic’’ for the case where there is no heating mechanism (e.g. conductive heating due to elastic scattering) other than the shock heating.

4 SELF-SIMILAR MODEL FOR SIDM HALOES IN THE MATTER-DOMINATED ERA

In this section we first show that formation and evolution of SIDM haloes in galactic scale are well approximated by self-similar equations. We then apply the fluid approximation to the problem and derive a set of ordinary differential equations. We will explain in detail how to solve these equations with proper boundary conditions.

4.1 Self-similarity of SIDM haloes

In §2.3, we described how a self-similar collapse model fits in cosmology by relating the logarithmic slope of the power spectrum, n , to the initial linear overdensity profile parametrized by ε . We, therefore, should first know what n is relevant to the problem we solve.

When collisionality of particles enters the system, its corresponding length scale comes into play, which in general does not grow in proportion to r_{ta} . Similarly, a new time scale will enter the system. However, we can still make the system self-similar after the addition of collisionality by some fine-tuning. The conductive heating term $\nabla \cdot \mathbf{f}$ enters the energy equation, and it should have the same time dependence as does the adiabatic change of the thermal energy, $\rho \frac{d}{dt} \left(\frac{3p}{2\rho} \right)$. Noting that $\rho \frac{d}{dt} \left(\frac{3p}{2\rho} \right) \propto r_{\text{ta}}^2 t^{-5}$ and $\nabla \cdot \mathbf{f} \propto r_{\text{ta}}^3 t^{-7}$, the condition

$$\xi = 2, \quad \varepsilon = \frac{1}{6} \quad (37)$$

preserves self-similarity of the system. This condition, $\varepsilon = 1/6$, is equivalent to $n = -2.5$, which can be seen from equation (6). The turnaround radius and mass grow in time as

$$r_{\text{ta}} \propto t^2, \quad M \propto t^4. \quad (38)$$

Now we find an intriguing coincidence. As described in §2.3, $n = -2.5$ is a good approximate value for haloes of galactic mass. SIDM haloes in galactic scales are, therefore, well described by self-similar equations. The following sections are dedicated to the detailed description of SIDM similarity solutions.

4.2 Basic equations and problem solving scheme

Under the condition of self-similarity, one can convert seemingly time-dependent equations into ordinary differential equations by properly scaling physical parameters. The turnaround radius r_{ta} is a natural choice for a length scale. With time t and the turnaround radius r_{ta} , we define dimensionless physical quantities – radius, velocity, density, pressure, mass and heat flux – as follows:

$$\lambda = r/r_{\text{ta}}, \quad (39)$$

$$V(\lambda) = v / \left(\frac{r_{\text{ta}}}{t} \right), \quad (40)$$

$$D(\lambda) = \rho / \rho_b, \quad (41)$$

$$P(\lambda) = p / \left[\rho_b \left(\frac{r_{\text{ta}}}{t} \right)^2 \right], \quad (42)$$

$$M(\lambda) = m / \left(\frac{4\pi}{3} \rho_b r_{\text{ta}}^3 \right), \quad (43)$$

$$F(\lambda) = f / \left[\rho_b \left(\frac{r_{\text{ta}}}{t} \right)^3 \right]. \quad (44)$$

Collapsing shells, which are assumed to be cold initially, obey Newton's law

$$\frac{d^2 r}{dt^2} = -\frac{Gm}{r^2} \quad (45)$$

where m is the mass enclosed by radius r . For the initial density perturbation defined by equation (1), this Newtonian motion can be described by a set of parametric equations, as follows (Abadi, Bower & Navarro 2000; see also Bertschinger 1985, for case of $\varepsilon = 1$):

$$\lambda = \sin^2(\theta/2) \left(\frac{\theta - \sin \theta}{\pi} \right)^{-\xi}, \quad (46)$$

$$V(\lambda) = \lambda \frac{\sin \theta (\theta - \sin \theta)}{(1 - \cos \theta)^2}, \quad (47)$$

$$D(\lambda) = \frac{9}{2} \frac{(\theta - \sin \theta)^2}{(1 - \cos \theta)^3 (1 + 3\epsilon\chi)}, \quad (48)$$

$$M(\lambda) = \lambda^3 \frac{9}{2} \frac{(\theta - \sin \theta)^2}{(1 - \cos \theta)^3}, \quad (49)$$

where $\chi = 1 - (3/2)(V(\lambda)/\lambda)$. Equations (46) - (49) therefore describe preshock motion.

The postshock motion of shells is described by full hydrodynamic equations. Equations (26), (27), (29), (32) and the definition of the infinitesimal mass $dm = 4\pi r^2 dr$ can be written with these dimensionless quantities as a set of ordinary differential equations:

$$(V - 2\lambda)D' + DV' + \frac{2DV}{\lambda} - 2D = 0, \quad (50)$$

$$(V - 2\lambda)V' + V = -\frac{P'}{D} - \frac{2M}{9\lambda^2}, \quad (51)$$

$$(V - 2\lambda) \left(\frac{P'}{P} - \frac{5D'}{3D} \right) = -\frac{10}{3} - \frac{2(F\lambda^2)'}{3P\lambda^2}. \quad (52)$$

$$F = -\frac{3ab}{2Q'} \left(a + \frac{2}{3Q'^2 P} \right)^{-1} \sqrt{\frac{P}{D}} \frac{d}{d\lambda} \left(\frac{P}{D} \right), \quad (53)$$

$$M' = 3\lambda^2 D, \quad (54)$$

where the prime indicates differentiation with respect to λ , and the nondimensional collisionality parameter Q' is defined as $Q' \equiv \sigma \rho_b r_{\text{ta}}$. We will later use a nondimensional constant $Q \equiv \sigma \rho_b r_s = \lambda_s Q'$, which is more directly related to the collision rate of an SIDM particle in a virialized structure with the shock radius r_s . For instance, the number of collisions a particle experiences in a time Δt is given by $N \equiv \sigma \rho v_{\text{rel}} \Delta t$ (e.g. Burkert 2000). The conversion of Q into N is straightforward:

$$N = \frac{\rho}{\rho_b} \frac{v_{\text{rel}} \Delta t}{r_s} Q = a \sqrt{\frac{p}{\rho}} \frac{\rho}{\rho_b} \frac{\Delta t}{r_s} Q. \quad (55)$$

Here we used the relation $v_{\text{rel}} = a\sqrt{p/\rho}$, where $a = 2.26$ again, which relates the average thermal velocity to the relative velocity for particles interacting elastically as hard spheres (equs. [7.10.13], [12.2.12] in Reif 1965).

Different solutions arise for different values of $Q(Q')$. To solve the coupled ordinary differential equations (equs. [50] - [54]), we need to connect the preshock values given

by equations (46) - (49 with $\xi = 2$) to the postshock values. This is described by the shock jump conditions (equs. [33], [34], and [36]) and the continuity of mass, which are expressed by nondimensional variables as

$$D_2 = \left(1 - \frac{2F_2}{P_2(V_1 - 2\lambda_s)} \right)^{-1} 4D_1, \quad (56)$$

$$P_2 = \left(\frac{3}{4} + \frac{F_2}{2P_2(V_1 - 2\lambda_s)} \right) D_1 (V_1 - 2\lambda_s)^2, \quad (57)$$

$$V_2 = 2\lambda_s + \left(1 - \frac{2F_2}{P_2(V_1 - 2\lambda_s)} \right) \frac{1}{4} (V_1 - 2\lambda_s), \quad (58)$$

$$M_2 = M_1, \quad (59)$$

where the subscript 1 denotes preshock values, while 2 denotes postshock values. Note that $P_1 = 0$ and $F_1 = 0$ because we assume cold infall. Note also that without terms containing F_2 , equations (56) - (59) are identical to the adiabatic jump conditions for $\gamma = 5/3$ gas (see equs. [6a] - [6d] in Abadi, Bower & Navarro 2000). These additional terms arise because of finite conductivity in the postshock region. Finally, the inner boundary conditions are

$$M(\lambda = 0) = 0, \quad (60)$$

$$V(\lambda = 0) = 0, \quad (61)$$

and

$$F(\lambda = 0) = 0. \quad (62)$$

In principle, the fluid equations (equs. [50] - [54]), preshock equations (equs. [46] - [49]), jump conditions (equs. [56] - [59]), and inner boundary conditions (equs. [60] - [62]) yield a unique solution. This solution was obtained numerically, by iteration, as follows. We arbitrarily chose the shock location λ_s (close to that of the adiabatic solution), central density $D(0)$ and central pressure $P(0)$. We then integrated differential equations from $\lambda = 0$ outward, using the LSODE (Livermore Solver for Ordinary Differential Equations), in which case variables behaved well. At the chosen shock location, we then obtained preshock values using the jump condition. If these values differed from those obtained from equations (46) - (49), we went back and chose a different λ_s , $D(0)$, and $P(0)$. We iterated this process until the jump condition was satisfied to a given error tolerance. This way we could get approximate solutions for several selected values of Q (listed in Table 1), all of which satisfied the shock jump conditions (equs. [56] - [59]) to less than 0.1% error. This was a very tedious and time-consuming job, but automation of the iterations made it possible to achieve this goal.

In practice we could not perform integration from $\lambda = 0$ because the differential equations have a coordinate singularity at the centre. Instead, we performed the integration from some small λ , using asymptotic forms for $\lambda \ll 1$: $D \simeq D(0)$, $P \simeq P(0)$, $V \simeq \frac{2}{3}\lambda$, $M \simeq D(0)\lambda^3$, and $F \simeq -\frac{5}{3}P(0)\lambda$.

5 RESULTS

We solved the coupled set of ordinary differential equations which yield the similarity solutions for SIDM haloes for the

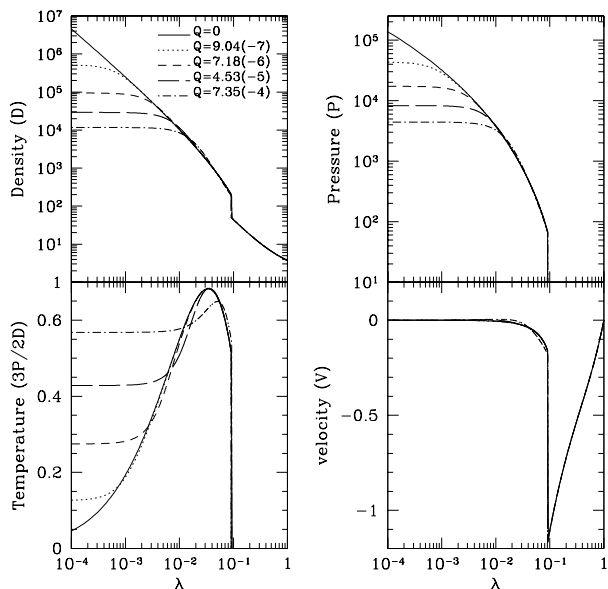


Figure 5. Similarity solution dimensionless profiles for low- Q regime. $Q = 0$ means “no conduction,” i.e. “adiabatic” post-shock gas. As Q increases, core density decreases and core temperature increases. Dimensionless similarity variables follow the definitions in Bertschinger (1985).

full range of values of the dimensionless collisionality parameter, Q . The results are plotted in Figures 5 and 6. Before we discuss the solutions for SIDM haloes with conduction ($Q \neq 0$), we begin with a description of the solution for $Q = 0$, the case without conduction. As we shall see, the latter yields a density profile which is in good agreement with the results of N-body simulations of haloes in the standard CDM model. We are justified, therefore, in applying the same self-similar infall model with $Q \neq 0$ to describe SIDM haloes.

Let us briefly describe the general properties of the SIDM similarity solutions and emphasize the importance of cosmological infall, before we describe the results in full detail.

5.1 Self-similar haloes without conduction ($\varepsilon = 1/6$): an analytical model for CDM N-body results

Before treating soft-core solutions, we describe properties of the adiabatic solution for $\varepsilon = 1/6$. As we shall show in what follows, the adiabatic infall solution for $\varepsilon = 1/6$ case resembles standard CDM haloes in many respects. First, it has a density cusp with a logarithmic slope $\simeq -1.27$ for $4 \times 10^{-3} < r/r_{200} < 1.4 \times 10^{-2}$, where r_{200} is the radius in which the average density is $200\rho_b$, if the density is extrapolated beyond r_s with the NFW profile that best-fits this adiabatic solution (Fig. 7). Note that it is possible to have a slope shallower than -2 because particle velocities are allowed to have a tangential component. If no tangential motion is allowed, the value -2 is the shallowest slope possible for collisionless dark matter haloes (Richstone & Tremaine 1984; Teyssier, Chieze & Alimi 1997; Bertschinger 1998).

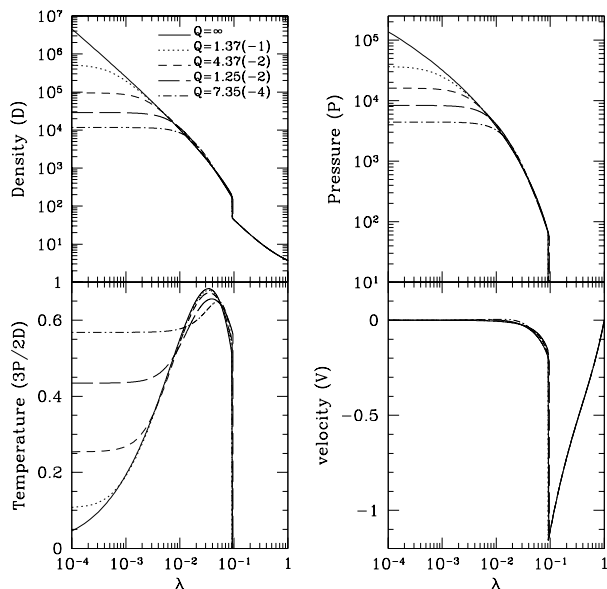


Figure 6. Similarity solution dimensionless profiles for the high- Q regime. Profiles are indistinguishable from those in Figure 5, even though the Q values are quite different. The effect of Q is reversed compared to the low- Q regime: as Q increases, core density increases and core temperature decreases.

Second, the temperature profile is very similar to that of CDM haloes. The temperature is zero at the centre, rises to a maximum at some λ , and then falls to a nonzero value at the shock. The most important part is that the temperature inversion exists. If not, the addition of conductivity will worsen the situation by initiating gravothermal catastrophe, rather than generating a soft core (Colín et al. 2002).

The average density inside the shock radius is found to be $564\rho_b$ for the adiabatic solution. This value is larger than the average density ($\simeq 200$) usually adopted by convention to identify virialized CDM haloes in N-body simulations. In terms of radius, $r_s = r_{564} \simeq 0.6r_{200}$. Our similarity solution, therefore, yields a shock at a smaller value of radius than is typically used to characterize the virial radius of CDM haloes in N-body simulations. However, as long as we focus on the properties inside r_{564} , the adiabatic solution is a good fit to CDM haloes as we shall see below. As seen in Figure 7, except for the innermost central region where the ambiguity of density slope exists between -1 (Navarro, Frenk & White 1997) and -1.5 (Moore et al. 1999), our adiabatic solution agrees with the NFW profile and the Moore profile to within 10%, depending on the concentration parameter. Compared to halo profiles studied by Diemand, Moore & Stadel (2004), the agreement is even better (Fig. [7]). We also find that a local logarithmic slope slowly changes to shallower values as one approaches the centre, which agrees with the trend reported by Navarro et al. (2004). We demonstrate this as follows.

We compare the adiabatic solution with the CDM N-body halo profiles mentioned above: i.e. the NFW profile,

$$\rho_{\text{NFW}} = \frac{\rho_{\text{sc}}}{(r/r_{\text{sc}})(1+r/r_{\text{sc}})^2}, \quad (63)$$

the Moore profile,

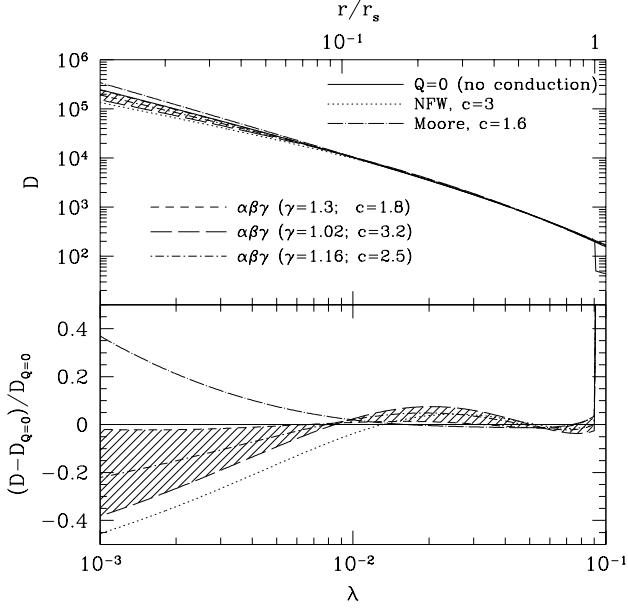


Figure 7. Comparison of self-similar halo profile without conduction with N-body results for CDM haloes: (top panel) Density (in units of cosmic mean density) vs. radius (in units of current turnaround radius) for similarity solution ($Q = 0$; $\varepsilon = 1/6$) (solid), the best-fitting NFW profile ($c = 3$), Moore profile ($c = 1.6$) and several $\alpha\beta\gamma$ profiles ($\alpha = 1$, $\beta = 3$) for different values of γ , $\gamma = 1.3$ (best fit), 1.02, 1.16, as labelled. Diemand, Moore & Stadel (2004) find N-body results for CDM haloes best fit by $(\alpha, \beta, \gamma) = (1, 3, \gamma = 1.16 \pm 0.14)$ (shaded region); (bottom panel) fractional deviation of the N-body results from similarity solution. Note that $\lambda = \lambda_s \simeq 0.09$ corresponds to $r_s = r_{564} \simeq 0.6 r_{200}$.

$$\rho_M = \frac{\rho_{sc}}{(r/r_{sc})^{1.5} (1 + (r/r_{sc})^{1.5})}, \quad (64)$$

and the $\alpha\beta\gamma$ profile (e.g. Diemand, Moore & Stadel 2004),

$$\rho_{\alpha\beta\gamma} = \frac{\rho_{sc}}{(r/r_{sc})^\gamma (1 + (r/r_{sc})^\alpha)^{(\beta-\gamma)/\alpha}}, \quad (65)$$

by finding the best-fitting parameters. The NFW and Moore profiles have two free parameters (ρ_{sc} and r_{sc}), while the $\alpha\beta\gamma$ profile has three (ρ_{sc} , r_{sc} , and γ) when α and β are fixed as in Diemand, Moore & Stadel (2004). We depict this comparison in Figure 7, with the “concentration parameter” – defined by $c \equiv r_{200}/r_{sc}$ – used to find the best-fitting N-body halo profiles. For $\alpha\beta\gamma$ profiles, we use the best-fitting profiles by Diemand, Moore & Stadel (2004), namely $\alpha = 1$, $\beta = 3$, $\gamma = 1.16 \pm 0.14$. Among these profiles, the $\alpha\beta\gamma$ profile with $\alpha = 1$, $\beta = 3$ and $\gamma = 1.3$ provides the best agreement with the adiabatic solution.

The relatively low concentration parameter, $c \simeq 3$, required for the best-fitting NFW profile deserves attention with respect to the cosmological mass accretion rate. This value is a bit small compared to the typical concentration parameters, $c \sim [4 - 20]$, observed at $z = 0$ in N-body simulations. Recent high resolution N-body simulation results, however, report such low concentration parameters if CDM haloes are observed at higher redshifts (e.g. Tasitsiomi et al. 2004). Individual haloes in CDM N-body simulations evolve over time, on average, through a contin-

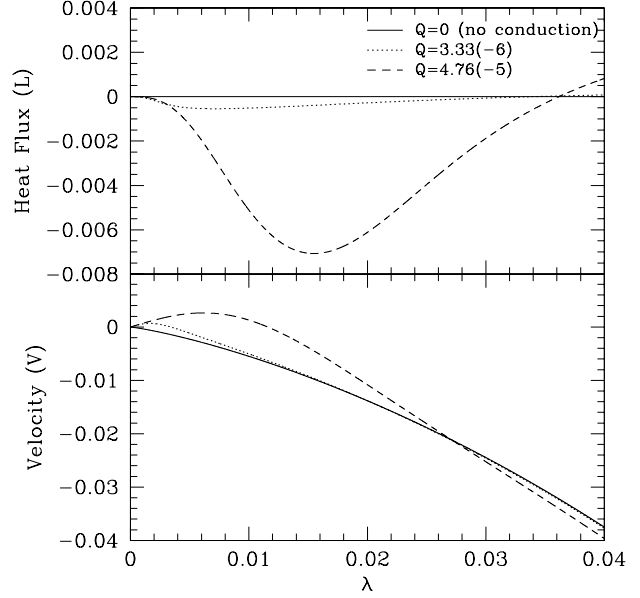


Figure 8. Profiles of heat flux and bulk velocity. Negative heat flux in the core indicates that heat is transferred from the halo to the core. The positive velocity bump indicates that the central density keeps being flattened by a net expansion of the core. Two different Q values were selected for comparison.

uous sequence of universal-shaped mass profiles of increasing total mass (Tasitsiomi et al. 2004; van den Bosch 2002; Wechsler et al. 2002). This Lagrangian mass evolution can be characterized by a universal mass accretion history:

$$M(a) = M_\infty \exp(-2a_f/a), \quad (66)$$

where a is the cosmic scale factor and a_f is some particular value of a , such as that at which $d \log M / d \log a = 2$ (Wechsler et al. 2002). As the mass of each halo grows with time due to the average effect of mergers and smooth infall, so does the concentration parameter c of its density profile, roughly as $c(a)/c(a_f) \propto a/a_f$ for $a/a_f > 1$ (Wechsler et al. 2002), after hovering at low values $c \approx 2 - 4$ during the initial phase of most rapid mass assembly prior to a_f (Tasitsiomi et al. 2004). Our similarity solution has $\frac{d \log M}{d \log a} = 6$, as seen in equation (38), and this corresponds to $a = a_f/3$. As our solution corresponds to a very early epoch in the halo formation history, or a fast accretion rate, such a low concentration parameter is a natural outcome.

In summary, we have shown that the adiabatic solution for $\varepsilon = 1/6$ approximates the N-body CDM halo profiles well, thus providing physical insights about their origin. In the following sections, we will describe SIDM halo solutions which arise as a result of non-zero conductivity.

5.2 Self-similar haloes with conduction ($\varepsilon = 1/6$): an analytical Model for SIDM haloes

5.2.1 Low- Q regime

We define the low- Q regime as $Q \leq Q_{th} = 7.35 \times 10^{-4}$. All the solutions have an isothermal, flat-density core, except for extremely small Q , where the system undergoes

Table 1. Central parameters and the shock location for different Q solutions. This table lists the whole range of Q .

Q	Q/Q_{th}	$D(0)$	$\frac{3P(0)}{2D(0)}$	λ_s
0	0	∞	0	9.0434(-2)
9.04(-7)	1.23(-3)	5.199(5)	1.258(-1)	9.0434(-2)
7.18(-6)	9.77(-3)	9.426(4)	2.747(-1)	9.0434(-2)
4.53(-5)	6.16(-2)	2.914(4)	4.289(-1)	9.060(-2)
7.35(-4)	1	1.169(4)	5.681(-1)	9.260(-2)
1.25(-2)	1.70(1)	2.882(4)	4.346(-1)	9.623(-2)
4.37(-2)	5.95(1)	9.515(4)	2.540(-1)	9.294(-2)
1.37(-1)	1.86(2)	5.199(5)	1.062(-1)	9.133(-2)
∞	∞	∞	0	9.0434(-2)

adiabatic collapse just as it would in the absence of SIDM conductivity. In this regime, as Q increases, the core density and pressure decrease. In other words, higher SIDM collisionality corresponds to a flatter core. This trend is also observed in the temperature profile. As Q increases, heat is more effectively transferred into the centre to equalize the temperature (Fig. [8]). Dependence of the central density, temperature and the location of the shock on Q is listed in Table 1 (see also Fig. [5]).

This regime roughly corresponds to the long mean free path limit. In this case, the heat flux is an increasing function of the SIDM cross section σ (eq. [31]). As an increase in Q is achieved by an increase in σ , the heat flux also increases correspondingly. In §5.3, a more detailed description will be given about the quantitative relation between the low(high)- Q regime to the long(short) mean free path limit.

In §5.5.2, we will also show that cosmological SIDM N-body simulations to date have been performed only in the low- Q regime. They see a monotonic behaviour of the halo profile depending on σ – as σ increases, core density decreases. In the next section, we will show that there is an additional regime, the high- Q regime, where this behaviour is reversed.

5.2.2 High- Q regime

In the high Q regime, solutions have $Q \geq Q_{\text{th}} = 7.35 \times 10^{-4}$. Once again, all the solutions have an isothermal, flat-density core, except for an extremely high Q case. In the high- Q regime, however, as Q (or σ) increases, the core density increases (Fig. [6]; Table 1), contrary to the behaviour observed for the low- Q regime. Therefore, Q_{th} gives the solution with the minimum possible core density $\rho_{\text{core}} \simeq 10^4 \rho_b$.

This behaviour occurs because the core of the halo is now in the short mean free path regime. In this case, contrary to the low- Q regime, the hybrid conduction term, equation (32), converges to the expression valid in the short mean free path limit, equation (30). An increase in Q or σ , therefore, results in a decrease in \mathbf{f} . Physically, the mean free path decreases as Q or σ increase, and it results in reducing the heat conduction.

For an extremely high Q (or σ), we found that the solution becomes identical to that of the adiabatic infall case. This result agrees qualitatively with the result by Yoshida et al. (2000a) and Moore et al. (2000), where they performed a smoothed particle hydrodynamics simulation, corresponding to the fluid limit of an infinite cross section.

What they found in haloes was a density cusp instead of a flat-density core. Quantitatively, our result does not fully agree with their result in which they find a profile even steeper than that of the collisionless case. As pointed out by Yoshida et al. (2000a), this may be attributed to the fact that small-scale shocks arise in the case of the fluid regime, thus increasing the entropy and ultimately steepening the central density. Our model is based upon an assumption that mass accretion is smooth and, therefore, cannot reproduce this effect.

5.3 Meaning of the collisionality parameter Q

We have showed that solutions are parametrized by the collisionality parameter Q , and also that there exist two regimes divided by a threshold value Q_{th} . To understand the physical meaning of Q , we now describe two relevant quantities: mean free path and the number of scatterings an SIDM particle experiences per Hubble time.

We first show that the ratio of the mean free path to the gravitational scale height (to be explained below) in the centre is very closely related to Q , and it provides a very clean explanation of the behaviour of the similarity solution. In previous sections, we explained the opposite trends observed in the two different regimes in terms of the heat flux \mathbf{f} (eq. [32]). The dependence of \mathbf{f} is determined by the ratio $\eta^2 \equiv (4\pi G/p)/(a\sigma^2)$: $\mathbf{f} \propto \sigma$ for $\eta^2 \gg 1$, and $\mathbf{f} \propto 1/\sigma$ for $\eta^2 \ll 1$. We find that, indeed, η is the ratio of two length scales, the mean free path and the gravitational scale height. The gravitational scale height (BSI),

$$H \equiv \sqrt{\sigma_v^2/(4\pi G\rho)} = \sqrt{p/(4\pi G\rho^2)}, \quad (67)$$

is a rough measure of the size of a given self-gravitating system, where σ_v^2 is the velocity dispersion – also note, however, that equation (67) determines the *local* gravitational scale height. In terms of the mean free path $\lambda_{\text{mfp}} \equiv 1/(\rho\sigma)$ and $a = 2.26$ as in equation (31), $\eta = \lambda_{\text{mfp}}/(\sqrt{a}H)$. We find that $\eta = 1$ at the centre for $Q = Q_{\text{th}}$. η at the centre monotonically increases as Q increases. The low- Q regime then corresponds to a condition $\eta > 1$, and the high- Q to a condition $\eta < 1$. Dependence of η on Q , as well as its radial variance, is plotted in Figure 9.

The number of scatterings that an SIDM particle experiences during the age of the universe, which we denote by N , is also an interesting quantity. As higher Q means more frequent scattering, N also shows a monotonic dependence on Q (Fig. [10]) as η does. According to equation (55), it can be shown that N is expressible in terms of dimensionless quantities as

$$N = N_{0,\text{th}} \sqrt{\frac{DP}{(DP)_{0,\text{th}}}} \left(\frac{Q}{Q_{\text{th}}} \right) = a\sqrt{DP}Q/\lambda_s, \quad (68)$$

where the subscript “0,th” refers to the value at $r = 0$ for $Q = Q_{\text{th}}$, and $N_{0,\text{th}} = 129$. It is interesting to see that $N_{0,\text{th}} \approx 100$ is required to achieve the maximal conductivity, namely $Q = Q_{\text{th}}$. We will handle the significance of this quantity in §5.5.2, when we compare our result to SIDM N-body simulation results.

Finally, we stress the importance of the radial variance of η and N . When $Q/Q_{\text{th}} \ll 1$ or $Q/Q_{\text{th}} \gg 1$, the system can be said, in a global sense, to reside in the long mean free path

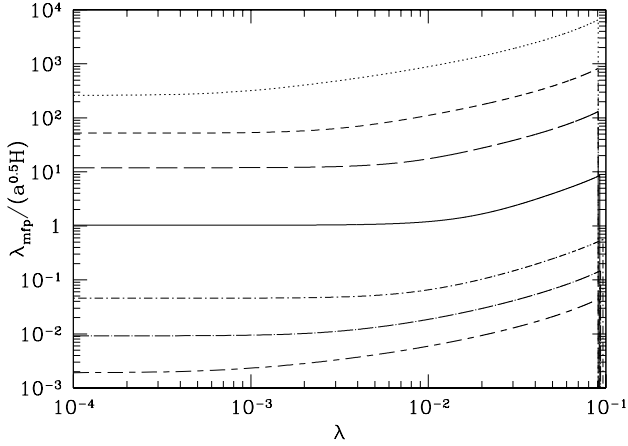


Figure 9. The parameter η versus dimensionless radius λ , where $\eta = \lambda_{\text{mfp}}/(\sqrt{a}H)$, the ratio of mean free path to gravitational scale height, for different values of Q . From top to bottom, each curve corresponds to $Q/Q_{\text{th}} = 1.23 \cdot 10^{-3}, 9.77 \cdot 10^{-3}, 6.16 \cdot 10^{-2}, 1, 17, 59.4,$ and 186 , respectively. The constant $a = 2.26$.

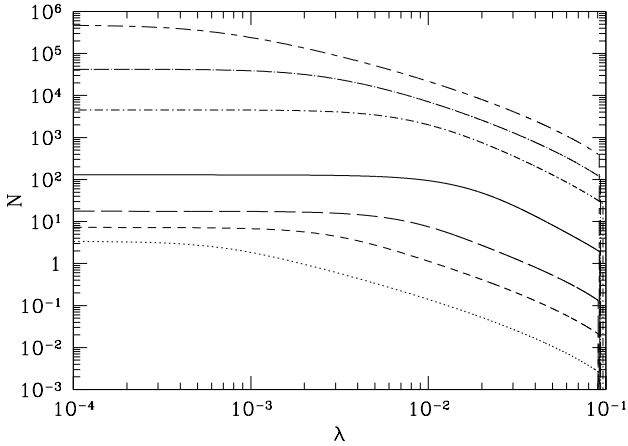


Figure 10. Number of scattering that an SIDM particle experiences during the age of the universe in dimensionless radius λ . From bottom to top, each curve corresponds to $Q/Q_{\text{th}} = 1.23 \cdot 10^{-3}, 9.77 \cdot 10^{-3}, 6.16 \cdot 10^{-2}, 1, 17, 59.4,$ and 186 , respectively.

limit or in the short mean free path limit, respectively. When $Q/Q_{\text{th}} \approx 1$, however, such a global definition is not valid. In the $Q = Q_{\text{th}}$ solution, for instance, $\eta = 1$ at the centre while $\eta \approx 10$ at the shock. N varies from ~ 100 at the centre to ~ 2 at the shock. This example shows that a global assumption of the short (or long) mean free path limit is not always valid, which requires a more careful attention when $Q \simeq Q_{\text{th}}$. We will handle this issue again in §6, with respect to the estimate on the ram-pressure stripping of substructure in a cluster environment made by Furlanetto & Loeb (2002) and Natarajan et al. (2002).

5.4 Importance of cosmological infall

The SIDM core grows in size as a fixed fraction of the turnaround radius, as guaranteed from the beginning because of the self-similarity of the system.

Therefore, this model shows that cosmological infall at a certain rate can completely inhibit the gravothermal catastrophe of the core by constantly pumping hot material into the halo (see Fig. [8]). This contradicts the prediction made in previous studies that the core would suffer gravothermal catastrophe in a Hubble time (e.g. Burkert 2000). Even when the infall rate is smaller than that required for our similarity solution ($M \propto t^4$), it will inhibit the core collapse to some extent. Only when the infall rate drops to a point where a system can be considered isolated will previous estimates of the timescale of collapse be valid. The net effect is a substantial delay of the collapse phase.

5.5 Application

5.5.1 Collisionality parameter as a function of σ and M

So far, we have described solutions in terms of Q . Now we seek a way to apply our solutions to practical problems. This is done by obtaining the dependence of Q on the scattering cross section σ and the mass of haloes M . From the Press-Schechter formalism, we find $Q = Q(\sigma, M)$ for “typical” haloes of mass M , which collapse when $\sigma_M = \delta_{\text{crit}}$ (σ_M is the standard deviation of the density fluctuations at the collapse epoch $z_{\text{coll}}(M)$ according to linear perturbation theory after the density field is filtered on the scale M ; δ_{crit} is the value of overdensity linearly extrapolated to a moment when the nonlinear overdensity becomes infinite.) Usually these are called $1-\sigma_M$ fluctuations.

As the $\varepsilon = 1/6$ adiabatic infall solution has a shock at r_{564} , the mass contained inside r_{564} , M_{564} , is smaller than M_{200} , which is typically quoted in the literature. In other words, the shock location is displaced from r_{200} substantially. As r_s is a function of M and z_{coll} , in order to get $Q = Q(M, z_{\text{coll}})$, we first should relate M_{564} to M . We therefore need a model whose density profile extends at least to r_{200} . We use the “truncated isothermal sphere” (TIS) model (Shapiro, Iliev & Raga 1999; Iliev & Shapiro 2001) for this purpose, for the following reasons: (1) it has a unique density profile, (2) all physical quantities are fully determined by the values of M and z_{coll} , (3) it has been proven to agree well with CDM prediction in many aspects (Shapiro & Iliev 2002), and (4) the average quantity (i.e. the average temperature) inside its own r_{564} is in a good agreement with that of our similarity solutions and of CDM N-body haloes⁸. We use a convenient set of formulae given by Iliev & Shapiro (2001) to get $r_s = r_{564}(M)$ for a given halo of mass M at its collapse epoch. In this model, the mass of the halo M is enclosed by the “truncation radius” r_t , given by

$$r_t = 187.2 \left(\frac{M}{10^{12} h^{-1} M_{\odot}} \right)^{1/3} \Omega_0^{-1/3} (1+z_{\text{coll}})^{-1} h^{-1} \text{kpc}, \quad (69)$$

⁸ We find the same level of agreement between our similarity solutions and the N-body haloes as was found between the TIS and N-body haloes in Shapiro, Iliev & Raga (1999, see the mass-temperature relation in § 8.4).

and we find that

$$M_{564} = 0.587M, \quad (70)$$

and

$$r_{564} = 0.514 r_t \\ = 96.22 \left(\frac{M}{10^{12} h^{-1} M_\odot} \right)^{1/3} \Omega_0^{-1/3} (1 + z_{\text{coll}})^{-1} h^{-1} \text{kpc}. \quad (71)$$

Note that M in this model is equivalent to M_{130} . Equations (69), (70), and (71) are valid only when the universe is in the matter-dominated era. The mean matter density is in general given by

$$\rho_b(z) = \Omega_0 \rho_{0,\text{crit}} (1+z)^3 = 1.88 \times 10^{-29} \Omega_0 (1+z)^3 h^2 \text{g/cm}^3. \quad (72)$$

When the scattering cross section σ is a constant, Q also remains constant in a matter-dominated era where $\rho_b \propto t^{-2}$ if $\varepsilon = 1/6$ (or $r_s \propto t^2$). From the equations above, we find that

$$Q = Q_{\text{th}} \left(\frac{\Omega_0}{0.27} \right)^{2/3} \left(\frac{\sigma}{218.5 \text{ cm}^2 \text{g}^{-1}} \right) \left(\frac{M}{10^{10} h^{-1} M_\odot} \right)^{1/3} \\ \times \left(\frac{h}{0.7} \right) \left(\frac{1 + z_{\text{coll}}}{1 + 2.09} \right)^2. \quad (73)$$

Note that typical ($1-\sigma_M$ fluctuation) haloes of $M = 10^{10} h^{-1} M_\odot$ collapse at $z_{\text{coll}} = 2.09$ in the currently-favoured Λ CDM universe with $h = 0.7$, $\Omega_0 = 0.27$, $\Omega_\Lambda = 0.73$ and $\sigma_8 = 0.9$. If we restrict the mass range of haloes such that the high mass end will still collapse in the matter-dominated era – $z_{\text{coll}} \gtrsim 1$ – and the low mass end roughly satisfies the self-similarity, we should choose haloes with masses $M \simeq [10^6 - 10^{12}] h^{-1} M_\odot$. In this mass range, equation (73) reads

$$Q \simeq [1.68 - 9.31] \times 10^{-4} \left(\frac{\sigma}{218.5 \text{ cm}^2 \text{g}^{-1}} \right) \quad (74)$$

for a Λ CDM universe (see Fig. [11]: for $\sigma = 218.5 \text{ cm}^2 \text{g}^{-1}$, $Q = 1.68 \times 10^{-4}$ corresponds to $M = 10^6 h^{-1} M_\odot$, while $Q = 9.31 \times 10^{-4}$ corresponds to $M = 10^{11.62} h^{-1} M_\odot$). Here we applied the Press-Schechter formalism to obtain $z_{\text{coll}}(M)$. However, just for comparison, we also calculated Q for haloes with $M \gtrsim 10^{12} h^{-1} M_\odot$, which typically have collapsed only recently. Such massive haloes must be rare, high- σ fluctuations in order to collapse by the present, and we cannot apply our similarity model to these haloes because their mass assembly deviates substantially from self-similar evolution. Note that the rarer the objects are, the higher the collapse redshift z_{coll} is, which in turn makes Q larger in equation (73). This trend can be seen in Figure 11.

5.5.2 Comparison with N-body simulation results

Consider the range of σ identified in the cosmological N-body simulation of SIDM by Davé et al. (2001): $\sigma = [0.56 - 5.6] \text{ cm}^2 \text{g}^{-1}$. In a Λ CDM universe, this range of σ in equation (74) then yields the range

$$Q \simeq [4.31 \times 10^{-7} - 2.39 \times 10^{-5}] \\ \simeq [5.86 \times 10^{-4} - 3.25 \times 10^{-2}] Q_{\text{th}} \quad (75)$$

for haloes with $10^6 h^{-1} M_\odot < M < 10^{12} h^{-1} M_\odot$. Here $Q = 4.31 \times 10^{-7}$ corresponds to $\sigma = 0.56 \text{ cm}^2 \text{g}^{-1}$ and

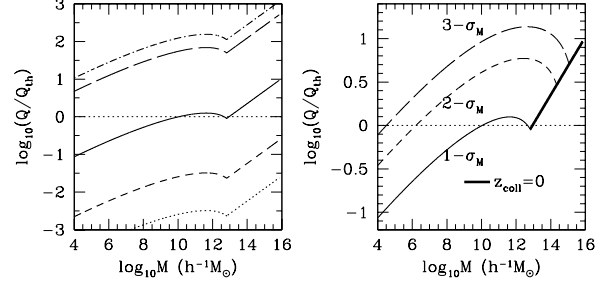


Figure 11. Left: Q vs. mass of haloes at their typical formation epoch for different σ . From bottom to top, curves correspond to $\sigma = 0.56, 5.6, 218.5, 1.2 \times 10^4, 2.7 \times 10^4$ respectively. They all correspond to $1-\sigma_M$ density peaks (σ_M means the standard deviation of the density fluctuations filtered on mass scale M at the collapse epoch); Right: Q vs. mass of haloes at their formation epoch for $\nu-\sigma_M$ ($\nu=1, 2, 3$) fluctuations with $\sigma = 218.5 \text{ cm}^2 \text{g}^{-1}$. Cluster-sized haloes observed at present will be clustered around the crossing point of the $3-\sigma_M$ line and $z_{\text{coll}} = 0$ line.

$M = 10^6 h^{-1} M_\odot$, while $Q = 2.39 \times 10^{-5}$ corresponds to $\sigma = 5.6 \text{ cm}^2 \text{g}^{-1}$ and $M = 10^{11.62} h^{-1} M_\odot$.

The simulation results of Davé et al. (2001) reside in the low- Q regime, as seen in equation (75). Our solutions allow us to identify a corresponding range of Q -values in the high- Q regime for which the density profiles are indistinguishable from their low- Q counterparts. The range of solutions described by equation (75) can be matched by solutions with

$$Q \simeq [1.37 \times 10^{-2} - 0.17] \simeq [18.6 - 231] Q_{\text{th}}, \quad (76)$$

or $\sigma \simeq [1.2 \times 10^4 - 2.7 \times 10^4] \text{ cm}^2 \text{g}^{-1}$. Here $Q = 1.37 \times 10^{-2}$ corresponds to $\sigma = 1.2 \times 10^4 \text{ cm}^2 \text{g}^{-1}$ and $M = 10^6 h^{-1} M_\odot$, while $Q = 2.7 \times 10^{-2}$ corresponds to $\sigma = 2.7 \times 10^4 \text{ cm}^2 \text{g}^{-1}$ and $M = 10^{12} h^{-1} M_\odot$.

Therefore, we predict that a cosmological N-body simulation of SIDM with $\sigma \simeq [1.2 \times 10^4 - 2.7 \times 10^4] \text{ cm}^2 \text{g}^{-1}$ will produce results similar to those of the Davé et al. (2001) simulations. The nondimensional core density $D(0)$ corresponding to the range of Q found in this section lies in the range $D(0) \simeq [3.3 \times 10^4 - 7.4 \times 10^5]$, while the nondimensional core temperature $T_{\text{core}} \equiv \frac{3P(0)}{2D(0)}$ is in the range $T_{\text{core}} \simeq [0.11 - 0.41]$. However, in order to obtain observationally acceptable values, we should actually fit the implied rotation curves of our similarity solutions directly to the empirical data. This is the main topic of §5.5.3.

5.5.3 Rotation curve fitting

In this section, we find best-fitting similarity solutions which match the observed rotation curves of dwarfs and LSBs. To do so, we simply compare our similarity solutions to an empirical fit by Burkert (1995). Burkert found that a density profile given by

$$\rho(r) = \frac{\rho_0 r_0^3}{(r + r_0)(r^2 + r_0^2)}, \quad (77)$$

where ρ_0 and r_0 are free parameters which represent the central density and a scale radius, respectively, matches halo density profiles which are derived from the observed rotation curves of dwarf galaxies. Recent studies of high-resolution

Table 2. Best-fitting concentration parameter of the Burkert profile and χ^2/ν . χ^2/ν is normalized by the value found for Q_{th} solution, $(\chi^2/\nu)_{Q_{\text{th}}} = 2.06 \times 10^{-4}$, the minimum.

Q/Q_{th}	$c_{564, \text{Burkert}}$	$(\chi^2/\nu)/(\chi^2/\nu)_{Q_{\text{th}}}$
0	5.51	4.72(2)
1.23(-3)	5.51	3.86(2)
9.77(-3)	5.49	1.36(2)
6.16(-2)	4.98	2.51(1)
1	3.95	1
1.70(1)	5.17	1.11(1)
5.95(1)	5.64	9.82(1)
1.86(2)	5.59	2.99(2)
∞	5.51	4.72(2)

$H\alpha$ rotation curves of dwarfs and LSBs confirm this result (Marchesini et al. 2002; see also references therein): they use a “hybrid” of $H\alpha$ and HI rotation curves which can extend from the centre to r_{max} , and find that the Burkert profile is the best fit for this range.

For fitting purposes, one should specify a radius where the circular velocity ($v = \sqrt{Gm/r}$) is the same for different halo models. In other words, local density may vary but the mass enclosed by such a radius – let us denote it by the “normalization radius” r_n – should be the same. We choose $r_n = r_{564}$, the “shock radius” of our similarity solutions, to find the best-fitting similarity solution to the Burkert profile. In this case, the “concentration parameter” $c_{564, \text{Burkert}} \equiv r_{564}/r_0$ is the only free parameter. The goodness of a fit is observed through the relative mean square deviation,

$$\chi^2/\nu \equiv \sum_i \left(\frac{v(r_i) - v_{\text{Burkert}}(r_i)}{v_{\text{Burkert}}(r_i)} \right)^2 / N, \quad (78)$$

where r_i is the radius of the i th data point and N is the number of such points.

We find that the solution with $Q = Q_{\text{th}}$ is best fit to the Burkert profile, as seen clearly in Figure 12 and Table 2^{9,10}. As shown in the right panel of Figure 12, when $Q = Q_{\text{th}}$, the SIDM halo rotation curve is virtually indistinguishable from the Burkert profile at all radii $r \leq r_{\text{max}}$, by contrast with the strong disagreement at small radii between the Burkert profile and the NFW and Moore profiles, respectively. Since the $Q = Q_{\text{th}}$ solution has the most effective conductivity, which is closest to an isothermal structure among the similarity solutions, we argue that dwarfs and LSBs described by the Burkert profile are systems which are almost fully

⁹ We find the same answer, that the Q_{th} solution is the best-fit to the Burkert profile, when we relax the constraint $r_n = r_{564}$ and assume that the two parameters, ρ_0 and r_0 , are both free.

¹⁰ The values of χ^2/ν shown in Table 2 show the relative quality of the fits of the Burkert profile to our self-similar SIDM profiles for different values of Q . In order to interpret these values in an absolute sense to determine if the fits are acceptable, we need to know the uncertainty of the fit of the Burkert profile to the observational data points. For example, if the $1-\sigma$ error bars are all a fraction f of the value of the data points, then the quantity $f^{-2}(\chi^2/\nu)$ should be small, i.e. $\lesssim 1$, for the theoretical curves to be a good fit at the $1-\sigma$ level. Since $(\chi^2/\nu)_{Q_{\text{th}}} = 2.06 \times 10^{-4}$, the SIDM profile for $Q = Q_{\text{th}}$ is a good fit to the data as long as $f \gtrsim 0.014$.

relaxed. This argument is supported by the fact that the TIS solution is almost identical to the Burkert profile (see Fig. [12]; also refer to Iliev & Shapiro 2001). The TIS solution is obtained by assuming that the system has a uniform temperature, isotropic random velocity, and the minimum possible energy, which in effect is equivalent to assuming a fully relaxed system. The solution with $Q = Q_{\text{th}}$ corresponds to the most relaxed system among our similarity solutions.

5.5.4 High value of σ : Contradiction with SIDM N-body simulation results?

An attempt to identify the range of SIDM cross section required to produce density profiles in agreement with dwarf galaxy rotation curves was previously made using N-body simulations of SIDM halo formation from Gaussian-random-noise cosmological density fluctuations (Davé et al. 2001; Yoshida et al. 2000b). These N-body results also indicated that, for this range of SIDM cross section, larger mass haloes (i.e. from the Milky Way to clusters) produce density profiles with flattened cores which are even more pronounced than those of dwarf galaxies. Since astronomical evidence suggests that such large haloes have relatively smaller cores, if any, than dwarf galaxies, this has led to the suggestion that the SIDM cross section must depend upon the relative velocity of the scattering events, decreasing with increasing velocity to suppress this effect in larger haloes (e.g. Colin et al. 2002). How do our self-similar solutions for SIDM halo formation compare with these N-body results?

The value of Q in the similarity solutions which best fits the dwarf galaxy rotation curves, Q_{th} , corresponds to a value of the SIDM cross section when we identify the halo mass and redshift to which we apply the similarity solution, as described above in § 5.5.1. For haloes of mass $M \simeq 10^{10} h^{-1} M_{\odot}$, which roughly represents the mass of dwarfs and LSBs observed, the solution with $Q = Q_{\text{th}}$ implies that $\sigma \simeq 218.5 \text{ cm}^2 \text{ g}^{-1}$, if the observed galaxies formed at the typical epoch for their mass scale (i.e. $1-\sigma_M$ fluctuations). This value is significantly larger than the range of acceptable cross section values reported for the N-body results for SIDM haloes by Davé et al. (2001) (equ. [75]) and similar results by Yoshida et al. (2000b).

Such discrepancy is observed also in N , the number of scatterings that an SIDM particle experiences during the age of the universe. Yoshida et al. (2000b) report that $N \simeq 1-10$ is enough to generate a soft core in their N-body SIDM haloes. We have seen in § 5.5.3, however, that $Q \approx Q_{\text{th}}$ is required to find acceptably flattened soft cores, and this in turn corresponds to $N \simeq 100$ in the core region as described in § 5.3.

We may attribute this discrepancy to the fact that Davé et al. (2001) did not actually perform rotation curve fitting with their N-body results. Davé et al. (2001) instead found their preferred value of σ by constraining the halo density at $r = 1 \text{ kpc}$ for haloes at the present epoch to be in the range $[0.01 - 0.1] M_{\odot} \text{ pc}^{-3}$. However, limited numerical resolution prevented them from determining the halo density at radii as small as those required to match the observed rotation curves which show flat-density cores. Our results suggest that, had their simulations been capable of resolving the profile at smaller radii, they would have found that the density continued to rise to a higher value

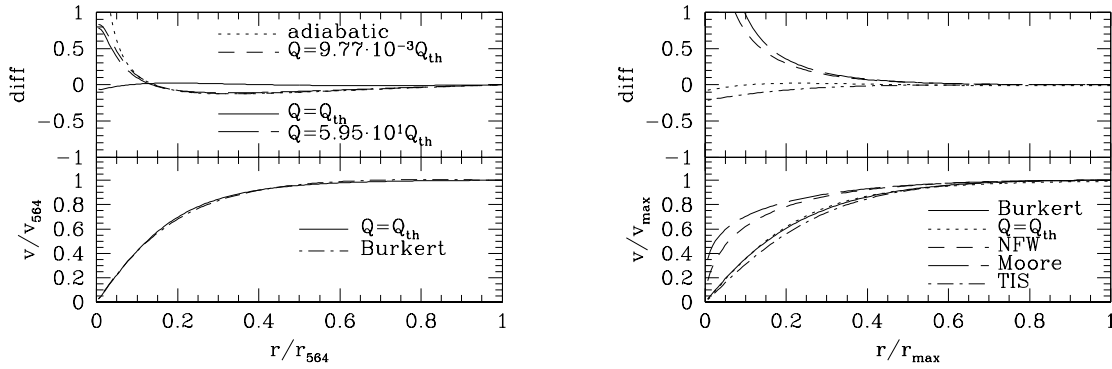


Figure 12. Rotation curve fitting. The upper left panel compares several different Q -solutions to the Burkert profile, normalized to r_{564} . The lower left panel shows the best-fitting solution to the Burkert profile, namely the Q_{th} solution. The right panel compares various halo models to the Burkert profile, normalized to r_{max} . It has the Q_{th} profile in r and v in units of $r_{\text{max,Burkert}} = 0.835 r_{564,\text{SIDM}}$ and $v_{\text{max,Burkert}} = 1.01 v_{564,\text{SIDM}}$, respectively, for the same profile as plotted in the lower left panel. In both boxes, the top panel shows the relative difference of a given profile, $(v - v_{\text{Burkert}})/v_{\text{Burkert}}$. The line types of the upper right panel follows the meaning of those in the lower right panel.

at smaller radii. As seen in Figure 1 of Davé et al. (2001), three haloes with $M \simeq 10^9 M_{\odot}$ ($M = (1.7, 0.9, 1.1)10^9 M_{\odot}$) are almost unaffected by the inclusion of SIDM collisionality if $\sigma \simeq [0.56 - 5.6] \text{ cm}^2 \text{ g}^{-1}$, which implies that the NFW-type cuspy profile persists in these haloes despite the SIDM interaction.

Conclusions drawn from current N-body simulations of SIDM halo profiles may, therefore, require revision in light of our results. The scattering cross-section $\sigma \simeq 218.5 \text{ cm}^2 \text{ g}^{-1}$ is in an interesting regime which has not been studied before by N-body simulations. This value may also help to resolve the problem identified by the N-body simulations for smaller cross section, in which larger-mass haloes result in relatively larger cores. The small cross section regime corresponds to $Q < Q_{\text{th}}$, for which the effect of SIDM conduction increases with increasing Q . As shown in Figure 11, larger-mass haloes typically have larger Q -values, since their larger sizes more than offset the lower mean densities which result from their later formation. According to our results, however, haloes from dwarf galaxies to clusters are not in the small cross section regime (i.e. low- Q regime). In fact, the dwarf galaxy rotation curves prefer $Q = Q_{\text{th}}$, so large mass galaxies and clusters have $Q > Q_{\text{th}}$, in general (see Fig. [11]). According to Figure 6, this high- Q regime suppresses conduction, yielding smaller cores (i.e. higher central densities) for higher-mass haloes. We predict, therefore, that as long as $\sigma \simeq 218.5 \text{ cm}^2 \text{ g}^{-1}$ is used in an SIDM N-body simulation, a constant value, independent of velocity, will suffice to match both dwarf galaxy rotation curves and the mass profiles of larger-mass haloes.

6 CONCLUSION/DISCUSSION

CDM particles have been assumed to be collisionless in the standard CDM theory of cosmic structure formation. Despite the success of this standard theory, the elementary particle physics theory necessary to explain the origin and

microscopic properties of the particles which comprise this dark matter is not yet known. It is natural for us to ask if the microscopic nature of CDM particles might lead to further constraints on this theory by astronomical observation. We have focused here on one such microscopic property, that of self-interaction by elastic scattering, and its effect on the internal structure and dynamical evolution of virialized CDM haloes during galaxy and large-scale structure formation. The apparent discrepancy between the observed density profiles of the haloes of dark-matter dominated dwarf and LSBs and those predicted by N-body simulations of collisionless CDM may well be resolved if one assumes that CDM particles interact with each other non-gravitationally. The self-interacting dark matter (SIDM) hypothesis is an attempt to produce such a nongravitational interaction between dark matter particles.

We have derived the first fully-cosmological similarity solutions for halo formation in the presence of collisionality. This provides an analytical theory of the effect of the self-interacting dark matter (SIDM) hypothesis on CDM halo density profiles as follows:

- We have adopted the spherical infall model of cosmological halo formation, guided by the results of N-body simulations of CDM. The collisional Boltzmann equation for the evolution of the gas of CDM particles yields a set of fluid-like conservation equations under the assumptions of spherical symmetry and isotropic velocity distribution. The effect of self-interaction collisions is accounted for by an effective conductivity term in the energy equation. This conductivity is valid for arbitrarily large or small collision mean free path λ_{mfp} .
- For an Einstein-de Sitter universe (or a flat universe with cosmological constant, at early times when matter dominates), the nonlinear growth of perturbations which leads to halo formation in the spherical infall model can be described by similarity solutions in the absence of conductivity. In the presence of SIDM conductivity, self-similarity

is still possible, but only for mass perturbations $\delta M/M \propto M^{-1/6}$. Remarkably, this self-similarity required in our solution is well-motivated and justified by the theory of halo formation from peaks of the Gaussian random noise density fluctuations (Hoffman & Shaham 1985). For galactic haloes, which form from density fluctuations whose power spectrum can be approximated by a power law $P(k) \propto k^{-2.5}$, the conditions required for this particular self-similarity naturally arise.

- According to our similarity solutions, collisions of SIDM transport heat from the hotter, outer halo region into the colder core region. This process flattens the central density, and continuous infall pumps energy into the halo which stabilizes the core against gravothermal catastrophe.

- These solutions are characterized by a single dimensionless quantity, the collisionality parameter $Q \equiv \sigma \rho_b r_{\text{vir}} \propto r_{\text{vir}}/\lambda_{\text{mfp}}$, where σ is the scattering cross section per unit mass, ρ_b is the mean matter density, r_{vir} is halo virial radius and λ_{mfp} is the collision mean free path. The maximum flattening of central density occurs for an intermediate value of Q , $Q_{\text{th}} = 7.35 \times 10^{-4}$, at which the halo is maximally relaxed to isothermality. The density profile of the Q_{th} solution matches that inferred from the observed rotation curves of dwarfs and low surface brightness galaxies (LSB) very well.

- In the low- Q regime ($Q < Q_{\text{th}}$), flattening of the central density profile becomes *stronger* as Q increases. Previous cosmological SIDM N-body simulations with $\sigma \simeq [0.1 - 10] \text{cm}^2 \text{g}^{-1}$ lie in this regime (Yoshida et al. 2000b, Davé et al. 2001, Colín et al. 2002). Central density profiles became flatter as they increased the scattering cross-section, which is equivalent to increase in Q , because $Q \propto \sigma$. On the contrary, in the high- Q regime ($Q > Q_{\text{th}}$), flattening of the central density becomes *weaker* as Q increases. This happens because the scattering mean free path becomes shorter as Q increases. SIDM simulations which adopt a fully collisional limit to derive the maximal density flattening, which corresponds to ordinary gas dynamics (Yoshida et al. 2000a; Moore et al. 2000), report that haloes obtain density profiles with central cusps as steep as or steeper than those in collisionless N-body simulations. This seemingly puzzling behaviour is easily explained: $\sigma \rightarrow \infty$ corresponds to $Q \rightarrow \infty$, and therefore density flattening becomes negligible.

- Under the assumption that dwarfs and LSBs formed at their typical collapse epoch in Λ CDM, $\sigma \simeq 200 \text{cm}^2 \text{g}^{-1}$ makes $Q = Q_{\text{th}}$, much higher than previous estimates, $\sigma \simeq [0.5 - 5] \text{cm}^2 \text{g}^{-1}$, based on N-body experiments. This value of σ , independent of halo mass, would make $Q > Q_{\text{th}}$ for clusters, which typically formed only recently, resulting in relatively less flattening of their central density profile and a smaller core. A velocity dependent cross-section, $\sigma \propto 1/v$, suggested by Yoshida et al. (2000b) is thus unnecessary.

- According to our similarity solutions, the solution for $Q = Q_{\text{th}}$ represents the solution most relaxed to isothermality inside the virialized postshock region. It is notable, therefore, that the $Q = Q_{\text{th}}$ solution is very similar to the non-singular TIS solution of Shapiro, Iliev & Raga (1999) for the post-collapse equilibrium structure of virialized haloes. The latter yields a mass profile almost indistinguishable from the mass profile of the Burkert fit to the rotation curves of dwarf and LSB galaxies (Iliev & Shapiro 2001), as is the $Q = Q_{\text{th}}$ SIDM profile we have derived here. This suggests that the TIS halo model, which assumes that haloes are isothermal,

is a natural outcome of the dynamical formation of CDM haloes when conductivity causes the halo to relax maximally toward isothermality.

One may improve upon this work by performing a cosmological N-body simulation. As our analysis is based upon self-similarity, or a constant mass accretion rate $\frac{\partial \log M}{\partial \log a} = 6$, when the mass accretion rate deviates from this canonical rate, our analysis is no longer valid. Several authors have investigated a realistic halo formation history both by an analytic approach and by N-body experiments, tracking the history of the “most massive progenitor (MMP)”. Wechsler et al. (2002) performed a cosmological N-body simulation and tracked the growth of MMP mass in a Λ CDM universe. Nusser & Sheth (1999) calculated the growth of MMP for a power-law power spectrum and van den Bosch (2002) calculated it for a CDM power spectrum, both using the extended Press-Schechter theory. These studies show that mass accretion starts with a fast, rapid merger and ends with smooth, continuous accretion. This trend is clearly seen in equation (66), where the logarithmic accretion rate is decreasing linearly with increasing scale factor a . The accretion rate obtained in this way is different from what is expected from HS. For $n = -2.5$ in the matter-dominated era, we find from equation (38) that $\frac{\partial \log M}{\partial \log t} = 4$ or $\frac{\partial \log M}{\partial \log a} = 6$. This fast accretion rate captures only the early mass accretion epoch given by equation (66), and therefore, one should not apply this rate to the later epoch when mass accretion becomes negligible. This is the moment where the evolution of SIDM haloes deviates from the self-similarity we assumed.

For cluster-mass haloes, there is another reason that our assumption of self-similarity breaks down and should be improved in future work; the value of n which enters the self-similar infall model in Λ CDM actually depends weakly upon halo mass. The value we have adopted to ensure self-similarity in the presence of SIDM collisionality, $n = -2.5$, is appropriate for the entire range of galactic halo masses. As Figure 3 shows, however, n increases with mass, and for clusters with mass above $10^{14} M_{\odot}$, $n > -2$. If $n \neq -2.5$, self-similarity is violated by the presence of SIDM terms in the equations. Since the accretion rate is lower if n is higher (i.e. $\frac{\partial \log M}{\partial \log a} = \frac{3}{n+3}$), the flattening effect of SIDM on the halo central density profile may be lower on cluster scales than expected from our self-similar solutions for $n = -2.5$.

Does our prediction of high value of σ , $\sigma \simeq 200 \text{cm}^2 \text{g}^{-1}$, affect the abundance of dark matter substructure? Gravitational lensing flux anomalies have been interpreted as evidence for the existence of dark matter substructures in the parent halo (Metcalf & Zhao 2002; Dalal & Kochanek 2002; Keeton, Gaudi & Petters 2003; Mao et al. 2004). The self-interacting dark matter, if real, would suppress the number of dark matter substructures to some extent. We are not sure at this stage, however, how strong this effect will be: the simple assumption of cold, continuous mass infall prevents us from making any strong prediction. We instead describe, in the following discussion, the complexity relating to two main mechanisms for suppressing the substructure formation when dark matter is collisional: ram-pressure stripping and thermal evaporation. One should also note that the interpretation of the lensing flux anomalies is not settled yet. Recent analysis indicates that this anomaly may not require

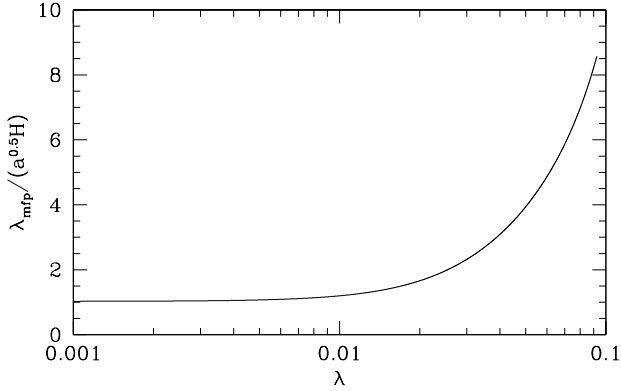


Figure 13. Comparison of length scales for the $Q = Q_{\text{th}}$ case. The mean free path λ_{mfp} is comparable to the gravitational scale height H in the core region. However, the ratio of the mean free path to the gravitational scale height becomes larger as the radius increases. See also Figure 9, which includes other values of Q .

any substructure in the primary lens halo, but only the substructure in the intergalactic space (Metcalf 2005).

We now point out some caveats found in previous analyses, which also require more realistic, cosmological analysis. As many previous analytical estimates have been based on either isolated haloes or very simplified models, we believe that fully cosmological N-body simulations in the high- Q (σ) regime should be carried out to clarify this issue. For instance, the restriction coming from the susceptibility of SIDM haloes to ram-pressure stripping (Furlanetto & Loeb 2002; Natarajan et al. 2002) may be relaxed if we remove the simplicity in their analysis. They determine the truncation radius of a galaxy in a cluster by the condition

$$\rho_c(r)v_g^2 = \rho_g(r_t)\sigma_g^2, \quad (79)$$

where v_g is the velocity of the galaxy inside a cluster, $\rho_c(r)$ is the density of the cluster at radius r , $\rho_g(r_t)$ is the density of the galaxy at its truncation radius r_t , and σ_g is the internal velocity dispersion of the galaxy. Equation (79) is valid for highly collisional fluid. They then use the restriction that

$$\frac{\lambda_{\text{mfp}}}{r_t} \simeq \frac{1}{\sigma \Sigma(r_t)} \leq 1 \quad (80)$$

where λ_{mfp} is the collision mean free path and $\Sigma(r_t)$, which is 0.024 g cm^{-2} for their fiducial case, is the surface density of a galaxy at r_t . However, this is a crude way of describing the fluid regime where the equation (79) can be applied. There exists a regime where the SIDM can be treated as collisional only at the centre because the ratio of the mean free path to the gravitational scale height becomes larger as the radius of a galaxy increases (see Fig. [13]; when we express these length scales with dimensionless terms used for our similarity solutions, the scattering mean free path is $L_{\text{mfp}} \equiv \frac{1}{DQ}$,

and the gravitational scale height is $H \equiv \frac{\sqrt{3P/2}}{D}$). In such cases, a ‘‘global’’ application of equation (79) is not valid. Ram-pressure stripping in this case would not be as severe as in the case of purely collisional fluid, because cluster SIDM particles have a high probability of penetrating an SIDM galactic halo deeply without experiencing collision at $r \gtrsim r_t$. Therefore, to apply equation (79), we have to be more

conservative in defining the fluid regime, which will relax the constraint $\sigma \lesssim 42 \text{ cm}^2 \text{ g}^{-1}$ (Natarajan et al. 2002) set by equation (80).

Gnedin & Ostriker (2001) constrained σ from their numerical and semi-analytical calculation of the evaporation time of elliptical galaxies embedded in a cluster environment. According to their analysis, such galactic haloes can evaporate within the age of the universe if $\sigma = [0.3 - 10^4] \text{ cm}^2 \text{ g}^{-1}$. However, their analysis is based on a fixed cluster environment. Consider a cosmological variant of this problem: for instance, an elliptical galaxy may form by a recent merger at $z = 1$ when the temperature of the cluster, which only forms at $z \simeq 0$, is very low. When the evaporation time is about the age of the universe ($\sim 10^{10} \text{ yr}$), the elliptical galaxy has a fair chance to survive because the evaporation time is greater than the time from its formation epoch to the present. The excluded range of σ would then change substantially by shifting the marginal values, $\sigma \simeq 0.3 \text{ cm}^2 \text{ g}^{-1}$ or $\sigma \simeq 10^4 \text{ cm}^2 \text{ g}^{-1}$, which correspond to the evaporation time of the order of the age of the universe. Moreover, their analysis is only valid for either the very long mean free path limit or the very short mean free path limit. They exclude the intermediate regime at $\sigma \simeq 200 \text{ cm}^2 \text{ g}^{-1}$ simply by an extrapolation of these two regimes.

Because of these problems, we assert that a more refined, fully cosmological analysis and new cosmological N-body simulations with a wider range of σ values, including $\sigma \simeq [100 - 500] \text{ cm}^2 \text{ g}^{-1}$, should be performed. Even though our analysis here is fully cosmological, it is restricted by the fact that it is based on a constant logarithmic mass accretion rate (i.e. $\frac{\partial \log M}{\partial \log a} = \frac{1}{\epsilon} = \frac{3}{n+3} = 6$ for $n = -2.5$) that provides self-similarity. However, a more realistic mass accretion history constructed from merger trees in N-body simulations shows a gradual decrease of the logarithmic mass accretion rate over time, as seen in equation (66) (e.g. Wechsler et al. 2002). When the mass accretion rate becomes very small at late times, the underlying halo properties will deviate significantly from self-similarity. Moreover, the relatively high scattering cross-section which we find provides the best-fitting to dwarf galaxy rotation curves – $\sigma \simeq 200 \text{ cm}^2 \text{ g}^{-1}$ – has never been tested in cosmological SIDM N-body simulations. We will explore these issues further in future work.

ACKNOWLEDGMENTS

We thank M. Alvarez, S. Shapiro, H. Martel, I. Iliev, and L. Chuzhoy for helpful discussions. This work was supported by NASA Astrophysical Theory Program grants NAG5-10825, NAG5-10826, NNG04G177G, and Texas Advanced Research Program grant 3658-0624-1999.

APPENDIX

We show how we got n_{eff} for different mass scales. It is slightly different from the usual way to obtain n_{eff} by differentiating the rms mass fluctuation, σ_M .

Typically, one has

$$n_{\text{eff}} = -3 \left(1 + \frac{d \ln \sigma_M^2}{d \ln M} \right) \quad (81)$$

where

$$\sigma_M^2 \equiv \frac{\langle (m - M)^2 \rangle}{M^2} = \frac{1}{2\pi^2} \int_0^\infty P(k)W^2(kR)k^2 dk, \quad (82)$$

where m is a mass enclosed by a sphere of radius R which also defines the *unperturbed* mass M through

$$M = \frac{4\pi}{3}R^3\rho_0, \quad (83)$$

where ρ_0 is the present matter density and the average $\langle \rangle$ is taken over all positions of the centre of these spheres. This “top-hat” filtering results in a window function

$$W(X) = \frac{3}{X}(\sin(X) - X \cos(X)). \quad (84)$$

It is then straightforward to calculate n_{eff} as a function of M using equation (81).

However, we are interested in the n_{eff} which is valid if one considers the initial average overdensity around density peaks, $\Delta_0(R)$ (HS). $\Delta_0(R)$ is given by

$$\Delta_0(R) \equiv \frac{\delta M}{M} = \frac{\delta_0}{\sigma^2} \frac{1}{2\pi^2} \int_0^\infty P(k)W(kR)k^2 dk, \quad (85)$$

where M and $W(X)$ are defined by equation (83) and (84), respectively. From equation (83) and equation (85), we can see that for a power-law power spectrum $P(k) \propto k^n$,

$$\Delta_0(R) \propto R^{-(n+3)} \propto M^{-(n+3)/3}. \quad (86)$$

Therefore, one can obtain n_{eff} as follows:

$$n_{\text{eff}} = -3 \left(1 + \frac{d \ln \Delta_0(M)}{d \ln M} \right). \quad (87)$$

The only difference in obtaining n_{eff} is then the power of the window function $W(X)$ in equations (82) and (85). One can therefore expect that there would be only a minor difference, which we confirmed (see Fig. [3]). We used the fitting formula for the transfer function by Eisenstein & Hu (1999), and worked in the Λ CDM concordance model with $\Omega_\Lambda = 0.73$, $\Omega_{m,0} = 0.27$, $h = 0.7$, $\sigma_8 = 0.9$ and untilted Harrison-Zel’dovich primordial power spectrum.

REFERENCES

- Abadi M. G., Bower R. G., Navarro J. F., 2000, MNRAS, 314, 759
- Ahn K., Shapiro P. R., 2003, J. Korean Astron. Soc., 36, 89; preprint (astro-ph/0212575)
- Ahn K., Shapiro P. R., 2003, RevMexAA(SC), 18, 1; preprint (astro-ph/0303058)
- Alvarez, M. A., Ahn K., Shapiro P. R., 2003, RevMexAA(SC), 18, 4; preprint (astro-ph/0302336)
- Avila-Rees V., Firmani C., Hernández X., 1998, ApJ, 505, 37
- Balberg S., Shapiro S. L., 2002, PRL, 88, 101301
- Balberg S., Shapiro S. L., Inagaki S., 2002, ApJ, 568, 475
- Bardeen J. M., Bond J. R., Kaiser N., Szalay A. S., 1986, ApJ, 304, 15
- Bertschinger E., 1985, ApJ, 58, 39
- Bertschinger E., 1989, ApJ, 340, 666
- Bertschinger E., 1998, Annu. Rev. Astro. Astrophys., 36, 599, §5.4
- Bettwieser E., 1983, MNRAS, 203, 811
- Binney J., Tremaine S., 1987, Galactic Dynamics, Princeton Univ. Press, Princeton, NJ
- Burkert A., 1995, ApJ, 447, L25
- Burkert A., 2000, ApJ, 534, L143
- Carlberg R. G. et al., 1997, ApJ, 485, L13
- Colín P., Klypin A. A., Kravtsov A. V., 2000, ApJ, 539, 561
- Colín P., Avila-Reese V., Valenzuela O., Firmani C., 2002, ApJ, 581, 777
- Dalal N., Kochanek C. S., 2002, ApJ, 572, 25D
- Davé R., Spergel D. N., Steinhardt P. J., Wandelt B. D., 2001, ApJ, 547, 574
- Del Popolo A., Gembara M., Recami E., Spedicato E., 2000, A&A, 353, 427
- Diemand J., Moore B., Stadel J., 2004, MNRAS, 353, 624
- Eisenstein D. J.; Hu W., 1999, ApJ, 511, 5
- El-zant A., Shlosman I., Hoffman Y., 2001, ApJ, 560, 636
- El-zant A., Hoffman Y., Primack J., Combes F., Shlosman I., 2004, ApJ, 607, L75
- Fillmore J. A., Goldreich P., 1984, ApJ, 281, 1
- Flores R. A., Primack J. R., 1994, ApJ, 427, L1
- Furlanetto S., Loeb A., 2002, ApJ, 565, 854
- Gnedin O. Y., Ostriker J. P., 2001, ApJ, 561, 61
- Gunn J. E., Gott J. R., 1972, ApJ, 176, 1
- Hayashi et al., 2004, MNRAS, 355, 794
- Hennawi J. F., Ostriker J. P., 2002, ApJ, 572, 41
- Hernquist L., 1990, ApJ, 356, 359
- Hiotelis N., 2002, A&A, 382, 84
- Hoffman Y., Shaham J., 1985, ApJ, 297, 16
- Holley-Bockelmann K., Weinberg M., Katz N., 2003, preprint (astro-ph/0306374)
- Hozumi S., Burkert A., Fujiwara T., 2000, MNRAS, 311, 377
- Iliev I. T., Shapiro P. R., 2001, MNRAS, 325, 468
- Keeton C. R., Gaudi B. S., Petters A. O., 2003, ApJ, 598, 138
- Kochanek C. S., White M., 2001, ApJ, 559, 531
- Kull A., 1999, ApJ, 516, L5
- Larson R. B., 1970, MNRAS, 147, 323
- Lokas E. L., Hoffman Y., 2000, ApJ, 542, L139
- Lynden-Bell D., Eggleton P. P., 1980, MNRAS, 191, 483
- Mao S., Jing Y., Ostriker J. P., Weller J., 2004, ApJ, 604, L5
- Marchesini D., D’Onghia E., Chincarini G., Firmani C., Concori P., Molinari E., Zacchei A., 2002, ApJ, 575, 801
- Metcalfe R. B., 2005, ApJ, 622, 72
- Metcalfe R. B., Zhao H., 2002, ApJ, 567, L5
- Moore B., Quinn T., Governato F., Stadel J., Lake G., 1999, MNRAS, 310, 1147
- Moore B., Gelato S., Jenkins A., Pearce F. R., Quilis V., 2000, ApJ, 535, L21
- Moore B., 2001, preprint (astro-ph/0103100)
- Natarajan P., Loeb A., Kneib J-P., Smail I., 2002, ApJ, 580, L17
- Navarro J. F., Eke V. R., Frenk C. S., 1996, MNRAS, 283, L72
- Navarro J. F., Frenk C. S., White S. M., 1997, ApJ, 490, 493
- Navarro et al., 2004, MNRAS, 349, 1039
- Nusser A., Sheth R. K., 1999, MNRAS, 303, 685

- Owen J. J., Weinberg D. H., Villumsen J. V., 1998, preprint (astro-ph/9805097)
- Primack J., 2003, preprint (astro-ph/0312549)
- Reif F., 1965, *Fundamentals of Statistical and Thermal Physics*, McGraw-Hill, New York
- Ryden B. S., Gunn J. E., 1987, *ApJ*, 318, 15
- Richstone D. O., Tremaine S., 1984, *ApJ*, 286, 27
- Shapiro P. R., Iliev I. T., 2002, *ApJ*, 565, L1
- Shapiro P. R., Iliev I. T., Raga A. C., 1999, *MNRAS*, 307, 203
- Shapiro P. R., Iliev I. T., Martel H., Ahn K., Alvarez M. A., 2005, preprint (astro-ph/0409173)
- Spergel D. N., Steinhardt P. J., 2000, *PRL*, 84, 3760
- Subramanian K., Cen R., Ostriker J. P., 2000, *ApJ*, 538, 528
- Tasitsiomi A., Kravtsov A. V., Gottlöber S., Klypin A. A., 2004, *ApJ*, 607, 125
- Teyssier R., Chieze J.-P., Alimi J.-M., 1997, *ApJ*, 480, 36
- Thomas P. A. et al., 1998, *MNRAS*, 296, 1061
- van den Bosch F. R., 2002, *MNRAS*, 331, 98
- van den Bosch F. R., Swaters R. A., 2001, *MNRAS*, 325, 1017
- Wechsler R. H., Bullock J. S., Primack J. R., Kravtsov A. V., Dekel A., 2002, *ApJ*, 586, 52
- Weinberg M. D., Katz N., 2002, *ApJ*, 580, 627
- Yoshida N., Springel V., White S. D. M., Tormen G., 2000a, *ApJ*, 535, L103
- Yoshida N., Springel V., White S. D. M., Tormen G., 2000b, *ApJ*, 544, L87
- Zentner A. R., Bullock J. S., 2002, *PRD*, 66, 043003